Vibration Analysis of Open Spherical Sandwich Panels with Soft Core Rested on an Elastic Foundation Subjected to Various Impulse Loads

Saman Sadripour, Raed Hadi Al Saffah, Ramazan-Ali Jafari-Talookolaei*, Reza Azadi

School of Mechanical Engineering, Babol Noshirvani University of Technology, Babol, Iran

* Corresponding author: ramazanali@gmail.com

Abstract

The study explores the behaviour of systems under both free and forced vibrations of spherical sandwich panels supported by an elastic foundation exposed to various impact load profiles. The panels consist of multilayer composite face sheets formulated based on the first-order shear deformation theory, and a soft core characterized by a higher-order theory employing in-plane displacement field of 3d-order and transverse displacement field of 2nd-order. By calculating the mechanical energy components, and introducing a nine-node higher-order element possessing 15 degrees of freedom per node, the element stiffness and mass matrices were determined. Boundary conditions are simulated through distributed virtual springs. A free vibration problem is evaluated to extract the structure's eigenfrequencies and mode shapes. Using the Newmark method, time response of displacement, velocity, acceleration, and phase planes are calculated for various impact profiles, specifically for half-sine pulses. This comprehensive analysis of sandwich panels' dynamic response under various impact loads reveals that the load profile critically determines structural behavior, essentially governing the boundary between safe operation and potential failure. For example, sudden loads like rectangular pulse emerged as the most critical case, causing extreme discontinuous responses across all dynamic parameters, and gradual loads (Gaussian/exponential) proved optimal for sensitive applications by generating smooth, controlled structural responses and providing ideal performance for stability-critical systems.

Keywords: Free Vibration; Transient Response; Sandwich Shell; Soft-Core; Finite Element Method (FEM).

1. Introduction

Sandwich structures are now improved compared to conventional monolithic metal structures owing to excellent mechanical properties relative to their weight, energy absorption, acoustic and thermal insulation, and corrosion resistance [1]. These multifunctional advantages have led them to find extensive application in aerospace engineering, shipbuilding, submarine construction, turbine blade manufacture, and biomedical applications [2, 3]. Therefore, it has become important to comprehend the behavior of sandwich structures comprehensively in order to enable optimum design. Among the different geometrical arrangements utilized in sandwich construction, curved shell structures exhibit better load-carrying capability than flat panels due to the curvature [4]. This mechanical benefit has made shells the element of choice in many mechanical systems and structural elements. These varied applications demonstrate the wide-ranging relevance of shell modelling and further emphasize the need for accurate predictions regarding the dynamic behavior of sandwich spherical panels, particularly for elastic foundation and impact-type excitations, as investigated in the current work.

Early investigations into the vibration behavior of spherical sandwich structures focused primarily on free vibration characteristics. Mirza and Singh [5] pioneered the field by analysing vibrational behavior of deep spherical sandwich structures featuring a thick core and two thin isotropic face sheets. in this paper Legendre functions was used and the results obtained using an iterative method. The influence of different variables including geometric and elastic properties was investigated in this paper. After that, Biglari and Jafari [6] utilized a higher-order sandwich panel theory to investigate the static behaviour and free vibration characteristics of doubly-curved shells featuring soft cores, employing Donnell's theory while neglecting core in-plane stress components. Hosseini-Hashemi et al. [7] derived

exact solutions capturing the in-plane and transverse (out-of-plane) vibration behaviour for spherical laminated shells with moderate thickness using Sanders' theory without approximations, decoupling Hamilton-derived equations through potential functions and employing both Navier and Lévy solution methods. Free vibration of sandwich spherical panels using FEM was analyzed by Sadripour et. al [8], the extended higher-order sandwich panel theory was utilized in this work, and How different parameters affect natural frequencies was studied.Le et al. [9] investigated the free vibration of functionally graded sandwich spherical panels. In this work, it was presumed that the structure was supported by a Kerr foundation. This analysis utilized an extension of the MITC4 element and the first order shear deformation theory was used because of its simplicity and efficiency and effect of various parameters was investigated.. The vibration behavior of spherical sandwich panels with a metal foam core and graphene platelet-reinforced composite face sheets on a Kerr foundation was analyzed by Ge et al. [10]. In this study, simply supported boundary conditions were assumed, and the equations were solved using an analytical approach. In 2025, Sahu and Kumar [11] studied static and vibrational behavior of doubly curved laminated composite shells including spherical shells utilizing the equivalent single layer approach using the Carrera Unified Formulation (CUF) framework to evaluate displacement fields, stress distributions, and natural frequencies. They presented their results using Finite element method.

In the field of forced vibration, In 1971, Culkowski and Reismann [12] studied the behavior of spherical sandwich shells in the presence of axisymmetric static and dynamic loading. In this study the membrane action of face sheets was only considered. After that, Kunukkasseril and Palaninathan [13] investigated the dynamic response of shallow spherical shells subjected to half-sine impact forces for several pulse duration. Sahan and Mehmet [14] proposed an alternative analytical method for analysing the transient vibrations of doubly-curved multilayer shells including spherical shells, under dynamic loads. The equations of motion were derived using the dynamic version of the virtual displacement method and the first-order shear deformation theory and Navier method. The study examined the effects of the number of layers, material properties, and shell geometry. Wang et al. [15] studied the transient response of a shallow doubly-curved composite shell reinforced with graphene sheets subjected to time-dependent blast loading. The equations of motion were formulated based on Hamilton's principle combined with the nonlinear von Kármán strain-displacement relationships. Guo et al. [16] conducted a dynamic analysis of doubly-curved multilayer composite shells with different boundary conditions using the domain decomposition method. Various numerical examples were considered to investigate the free vibrations, steady-state vibrations, and transient responses of doubly-curved composite shells with different geometries and material properties under external forces. In a study by Dogan [17], the dynamic performance of multilayer composite shells under diverse impact loadings was explored. By utilizing Hamilton's principle, the equations of motion were formulated and subsequently solved using the Navier method.The (1+z/R) term was included to account for curvature effects. Kareem and Majeed [18] numerically and experimentally evaluated the transient dynamics of shallow laminated spherical shells under external object impact. A new higher-order theory was used for analytical modelling, and the results were validated against experimental data. Also, Katariya and Panda [19] analysed the static displacement, dynamic frequency response, and time-dependent behaviour of a sandwich shells subjected to a variety of mechanical loads. Subramani et al. [20] studied the free and forced vibration responses of CNT-reinforced composite spherical sandwich shells using a higher-order shear deformation model. The formulation was solved using an element with nine nodes, where each node has nine degrees of freedom The forced vibration of a sector of spherical sandwich shells under the effect of low velocity impact was investigated by Raissi [21] using a layer wise higher-order shear deformation theory. In this study the face sheets were considered to be piezoelectric and the core was made of functionally graded carbon nanotubes. The natural characteristics of elastic sandwich spherical shells under radial excitation were studied by Liu and Wang [22] through wave propagation analysis. In their work, they determined the natural frequencies for structures with free-free and clamped-clamped boundary supports. In 2025, the free vibration and transient response of auxetic honeycomb doubly curved sandwich shells, including spherical ones, rested on visco-pasternak foundation subjected to low-velocity impact load was studied by Thi [23] using finite element method based on higher order shear deformation theory. Prior investigations into sandwich panels have largely dealt with planar or singly curved configurations, often ignoring the mutual impacts of curvature,, foundation interaction, and realistic boundary conditions. In our prior work (Sadripour et al. [24]), the dynamic response of open panels with double curvature under a uniformly moving load was investigated without considering the presence of an elastic foundation or impact-type loading. In the current research, a thorough vibrational investigation of spherical sandwich panels supported by elastic foundations, exposed to a range of transient impact loads, was considered. By addressing these combined effects, the current study aims to offer a more accurate and generalised understanding of the vibrational behaviour of curved sandwich panels under dynamic impact environments.

2. Mathematical formulations

In this section, the problem's mathematical modelling approach is presented. To this end, a spherical sandwich shell, as illustrated in Figure 1, is considered. As demonstrated, a curvilinear coordinate framework is employed to describe the problem configuration, in which α denotes the longitudinal coordinate, β the latitudinal coordinate, and z the coordinate across the thickness. It is considered that this global coordinate system is positioned at the shell's mid-surface. Three main layers compromise the structure: a soft-core layer enclosed by two multilayered composite face sheets. a, b, and h denote the length, the width and total thickness of the shell, where $h = h_t + h_c + h_b$. Throughout this study, the subscripts t, c, and b are assigned to the top face sheet, the core, and the bottom face sheet, in that order. Additionally, *F* represents the external force applied to the shell.

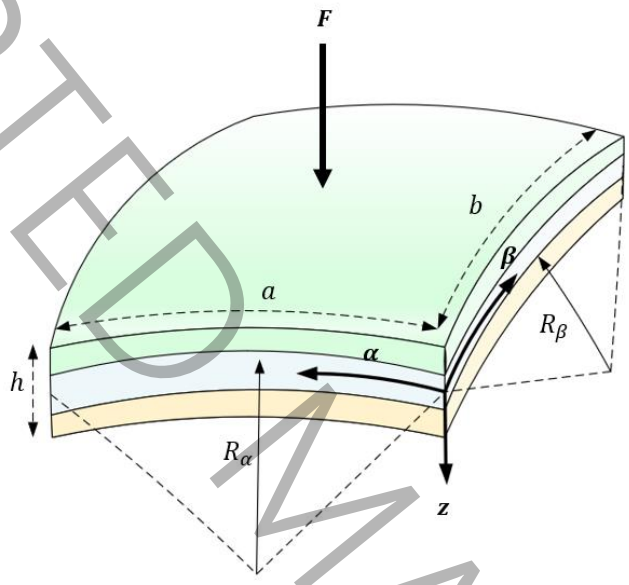

Figure 1. Schematic of the sandwich panel

In this study, to model the softness of the core, the Extended High-Order Sandwich Panel Theory (EHSAPT) is employed [25]. In this formulation, the face sheets are described through FSDT, while the core is described through a high-order displacement field derived from the three-dimensional elasticity solution. Accordingly,

For face sheets:

$$\mathbf{u}_f(\alpha,\beta,z_f,t) = \begin{Bmatrix} u_f(\alpha,\beta,z_f,t) \\ v_f(\alpha,\beta,z_f,t) \\ w_f(\alpha,\beta,z_f,t) \end{Bmatrix} = \begin{Bmatrix} u_0^f(\alpha,\beta,t) + z_f\psi_\alpha^f(\alpha,\beta,t) \\ v_0^f(\alpha,\beta,t) + z_f\psi_\beta^f(\alpha,\beta,t) \\ w_0^f(\alpha,\beta,t) \end{Bmatrix} \quad , \quad f = t,b \tag{1}$$

And for the core:

$$\mathbf{u}_c = (\alpha,\beta,z_c,t) = \begin{Bmatrix} u_c(\alpha,\beta,z_c,t) \\ v_c(\alpha,\beta,z_c,t) \\ w_c(\alpha,\beta,z_c,t) \end{Bmatrix} = \begin{Bmatrix} u_0(\alpha,\beta,t) + z_c u_1(\alpha,\beta,t) + z_c{}^2 u_2(\alpha,\beta,t) + z_c{}^3 u_3(\alpha,\beta,t) \\ v_0(\alpha,\beta,t) + z_c v_1(\alpha,\beta,t) + z_c{}^2 v_2(\alpha,\beta,t) + z_c{}^3 v_3(\alpha,\beta,t) \\ w_0(\alpha,\beta,t) + z_c w_1(\alpha,\beta,t) + z_c{}^2 w_2(\alpha,\beta,t) \end{Bmatrix} \tag{2}$$

To compute the strain components of the structure, we have:

$$\boldsymbol{\varepsilon} = \mathbf{B}\mathbf{u} \tag{3}$$

With $\boldsymbol{\varepsilon}$ is the vector of structural strains, $\mathbf{u}$ denotes the displacement vector, while $\mathbf{B}$ represents the strain–displacement gradient matrix, which is influenced by the structural geometry. Assuming linear strain–displacement relations for the spherical panel, we have:

$$\begin{Bmatrix} \varepsilon_\alpha \\ \varepsilon_\beta \\ \varepsilon_z \\ \gamma_{\alpha\beta} \\ \gamma_{\alpha z} \\ \gamma_{\beta z} \end{Bmatrix} = \begin{bmatrix} \frac{1}{(1+z/R)}\frac{\partial}{\partial\alpha} & 0 & \frac{1}{R(1+z/R)} \\ 0 & \frac{1}{(1+z/R)}\frac{\partial}{\partial\beta} & \frac{1}{R(1+z/R)} \\ 0 & 0 & \frac{\partial}{\partial z} \\ \frac{1}{(1+z/R)}\frac{\partial}{\partial\beta} & \frac{1}{(1+z/R)}\frac{\partial}{\partial\alpha} & 0 \\ \frac{\partial}{\partial z}-\frac{1}{R(1+z/R)} & 0 & \frac{1}{(1+z/R)}\frac{\partial}{\partial\alpha} \\ 0 & \frac{\partial}{\partial z}-\frac{1}{R(1+z/R)} & \frac{1}{(1+z/R)}\frac{\partial}{\partial\beta} \end{bmatrix} \begin{Bmatrix} u \\ v \\ w \end{Bmatrix} \tag{4}$$

By substituting the displacement fields (1) and (2) into the above relation, the strain–displacement equations may be expressed separately for each layer. These equations are presented in detail in references [26, 27]. By determining the strains, the structural stresses can be obtained using the following constitutive relation:

$$\boldsymbol{\sigma} = \mathbf{Q}\boldsymbol{\varepsilon} \tag{5}$$

Where $\boldsymbol{\sigma}$ represents the stress vector and $\mathbf{Q}$ denotes the constitutive matrix, which depends on the material characteristics for each layer. Considering orthotropic properties, one can express the stress-strain relations as follows for a typical k^{th} lamina:

$$\begin{Bmatrix} \sigma_\alpha^k \\ \sigma_\beta^k \\ \tau_{\alpha\beta}^k \end{Bmatrix} = \begin{bmatrix} \overline{Q}_{11}^k & \overline{Q}_{12}^k & \overline{Q}_{16}^k \\ \overline{Q}_{12}^k & \overline{Q}_{22}^k & \overline{Q}_{26}^k \\ \overline{Q}_{16}^k & \overline{Q}_{26}^k & \overline{Q}_{66}^k \end{bmatrix} \begin{Bmatrix} \varepsilon_\alpha^k \\ \varepsilon_\beta^k \\ \gamma_{\alpha\beta}^k \end{Bmatrix}$$
$$\begin{Bmatrix} \tau_{\beta z}^k \\ \tau_{\alpha z}^k \end{Bmatrix} = \begin{bmatrix} \overline{Q}_{44}^k & \overline{Q}_{45}^k \\ \overline{Q}_{45}^k & \overline{Q}_{55}^k \end{bmatrix} \begin{Bmatrix} \gamma_{\beta z}^k \\ \gamma_{\alpha z}^k \end{Bmatrix} \tag{6}$$

In which $\overline{Q}_{ij}^k$ are transformed reduced stiffness terms which are defined as follows:

$$\begin{bmatrix} \overline{Q}_{11}^k & \overline{Q}_{12}^k & 0 & 0 & 0 \\ \overline{Q}_{12}^k & \overline{Q}_{22}^k & 0 & 0 & 0 \\ 0 & 0 & \overline{Q}_{66}^k & 0 & 0 \\ 0 & 0 & 0 & \overline{Q}_{44}^k & 0 \\ 0 & 0 & 0 & 0 & \overline{Q}_{55}^k \end{bmatrix} = [T]^{-1} \begin{bmatrix} Q_{11}^k & Q_{12}^k & 0 & 0 & 0 \\ Q_{12}^k & Q_{22}^k & 0 & 0 & 0 \\ 0 & 0 & Q_{66}^k & 0 & 0 \\ 0 & 0 & 0 & Q_{44}^k & 0 \\ 0 & 0 & 0 & 0 & Q_{55}^k \end{bmatrix} [T] \tag{7}$$

where Q_{ij}^k for k^{th} layer are presented as follows:

$$Q_{11}^k = \frac{E_1^k}{1-\nu_{12}^k \nu_{21}^k} \quad , \quad Q_{12}^k = \frac{\nu_{12}^k E_2^k}{1-\nu_{12}^k \nu_{21}^k}$$
$$Q_{22}^k = \frac{E_2^k}{1-\nu_{12}^k \nu_{21}^k} \quad , \quad Q_{44}^k = G_{23}^k \quad , \quad Q_{55}^k = G_{13}^k \quad , \quad Q_{66}^k = G_{12}^k \tag{8}$$

in which ν^k, E^k, and G^k are, Poisson's ratio, modulus of elasticity and shear modulus of k^{th} layer, respectively and T is transformed matrix and defined as:

$$T = \begin{bmatrix} m^2 & n^2 & 2mn & 0 & 0 \\ n^2 & m^2 & -2mn & 0 & 0 \\ -mn & mn & m^2-n & 0 & 0 \\ 0 & 0 & 0 & m & n \\ 0 & 0 & 0 & -n & m \end{bmatrix} \tag{9}$$

In which $m = \cos\theta^k$, $n = \sin\theta^k$, and θ^k is the orientation angle of fibres with respect to the principal axis of k^{th} lamina. The top and bottom face sheet stress resultants are defined as:

$$\begin{bmatrix} N_\alpha^i \\ N_{\alpha\beta}^i \\ Q_\alpha^i \end{bmatrix} = \sum_{k=1}^{N^i} \int_{z_{i_{k-1}}}^{z_{i_k}} \begin{bmatrix} \sigma_\alpha^i \\ \sigma_{\alpha\beta}^i \\ \sigma_{\alpha z}^i \end{bmatrix} (1+\frac{z_i}{R^i}) dz_i$$
$$\begin{bmatrix} N_\beta^i \\ N_{\beta\alpha}^i \\ Q_\beta^i \end{bmatrix} = \sum_{k=1}^{N^i} \int_{z_{i_{k-1}}}^{z_{i_k}} \begin{bmatrix} \sigma_\beta^i \\ \sigma_{\alpha\beta}^i \\ \sigma_{\beta z}^i \end{bmatrix} (1+\frac{z_i}{R^i}) dz_i \tag{10}$$
$$\begin{bmatrix} M_\alpha^i \\ M_{\alpha\beta}^i \end{bmatrix} = \sum_{k=1}^{N^i} \int_{z_{i_{k-1}}}^{z_{i_k}} \begin{bmatrix} \sigma_\alpha^i \\ \sigma_{\alpha\beta}^i \end{bmatrix} z_i (1+\frac{z_i}{R^i}) dz_i$$
$$\begin{bmatrix} M_\beta^i \\ M_{\beta\alpha}^i \end{bmatrix} = \sum_{k=1}^{N^i} \int_{z_{i_{k-1}}}^{z_{i_k}} \begin{bmatrix} \sigma_\beta^i \\ \sigma_{\alpha\beta}^i \end{bmatrix} z_i (1+\frac{z_i}{R^i}) dz_i$$

By utilizing equations (3) and (5), the above relation can be replaced by the following expression:

$$\begin{Bmatrix} N_\alpha^i \\ N_\beta^i \\ N_{\alpha\beta}^i \\ N_{\beta\alpha}^i \\ M_\alpha^i \\ M_\beta^i \\ M_{\alpha\beta}^i \\ M_{\beta\alpha}^i \end{Bmatrix} = \begin{bmatrix} A_{11}^i & A_{12}^i & A_{16}^i & A_{16}^i & B_{11}^i & B_{12}^i & B_{16}^i & B_{16}^i \\ A_{12}^i & A_{22}^i & A_{26}^i & A_{26}^i & B_{12}^i & B_{22}^i & B_{26}^i & B_{26}^i \\ A_{16}^i & A_{26}^i & A_{66}^i & A_{66}^i & B_{16}^i & B_{26}^i & B_{66}^i & B_{66}^i \\ A_{16}^i & A_{26}^i & A_{66}^i & A_{66}^i & B_{16}^i & B_{26}^i & B_{66}^i & B_{66}^i \\ B_{11}^i & B_{12}^i & B_{16}^i & B_{16}^i & C_{11}^i & C_{12}^i & C_{16}^i & C_{16}^i \\ B_{12}^i & B_{22}^i & B_{26}^i & B_{26}^i & C_{12}^i & C_{22}^i & C_{26}^i & C_{26}^i \\ B_{16}^i & B_{26}^i & B_{66}^i & B_{66}^i & C_{16}^i & C_{26}^i & C_{66}^i & C_{66}^i \\ B_{16}^i & B_{26}^i & B_{66}^i & B_{66}^i & C_{11}^i & C_{11}^i & C_{11}^i & C_{11}^i \end{bmatrix} \begin{Bmatrix} \varepsilon_{0\alpha}^i \\ \varepsilon_{0\beta}^i \\ \varepsilon_{0\alpha\beta}^i \\ \varepsilon_{0\beta\alpha}^i \\ \kappa_\alpha^i \\ \kappa_\beta^i \\ \kappa_{\alpha\beta}^i \\ \kappa_{\beta\alpha}^i \end{Bmatrix} \quad , \quad i = t, b \tag{11}$$

$$\begin{Bmatrix} Q_\alpha^i \\ Q_\beta^i \end{Bmatrix} = k_s \begin{bmatrix} \overline{A}_{55}^i & A_{45}^i \\ A_{45}^i & A_{44}^i \end{bmatrix} \begin{Bmatrix} \gamma_{0\alpha z}^i \\ \gamma_{0\beta z}^i \end{Bmatrix}$$

In which k_s is the shear correction factor, which is taken to be 5/6, and:

Where shear correction factor is considered to be $k_s = 5/6$. And:

$$(A_{mn}^i, B_{mn}^i, C_{mn}^i) = \sum_{k=1}^{N^i} \overline{Q}_{mn}^k \int_{z_{i_{k-1}}}^{z_{i_k}} (1, z_i, {z_i}^2) dz_i \quad , \quad i = t, b \tag{12}$$

In a similar manner, for the core:

$$\begin{Bmatrix} N_\alpha \\ N_\beta \\ N_{\alpha\beta} \\ N_{\beta\alpha} \\ M_{1\alpha} \\ M_{1\beta} \\ M_{1\alpha\beta} \\ M_{1\beta\alpha} \\ M_{2\alpha} \\ M_{2\beta} \\ M_{2\alpha\beta} \\ M_{2\beta\alpha} \\ M_{3\alpha} \\ M_{3\beta} \\ M_{3\beta\alpha} \\ M_{3\beta\alpha} \end{Bmatrix} = \begin{bmatrix} A_{11} & A_{12} & A_{16} & A_{16} & B_{11} & B_{12} & B_{16} & B_{16} & C_{11} & C_{11} & C_{11} & C_{11} & D_{11} & D_{12} & D_{16} & D_{16} \\ A_{12} & A_{22} & A_{26} & A_{26} & B_{12} & B_{22} & B_{26} & B_{26} & C_{12} & C_{22} & C_{26} & C_{26} & D_{12} & D_{22} & D_{26} & D_{26} \\ A_{16} & A_{26} & A_{66} & A_{66} & B_{16} & B_{26} & B_{66} & B_{66} & C_{16} & C_{26} & C_{66} & C_{66} & D_{16} & D_{26} & D_{66} & D_{66} \\ A_{16} & A_{26} & A_{66} & A_{66} & B_{16} & B_{26} & B_{66} & B_{66} & C_{16} & C_{26} & C_{66} & C_{66} & D_{16} & D_{26} & D_{66} & D_{66} \\ B_{11} & B_{12} & B_{16} & B_{16} & C_{11} & C_{12} & C_{16} & C_{16} & D_{11} & D_{12} & D_{16} & D_{16} & E_{11} & E_{12} & E_{16} & E_{16} \\ B_{12} & B_{22} & B_{26} & B_{26} & C_{12} & C_{22} & C_{26} & C_{26} & D_{12} & D_{22} & D_{26} & D_{26} & E_{12} & E_{22} & E_{26} & E_{26} \\ B_{16} & B_{26} & B_{66} & B_{66} & C_{16} & C_{26} & C_{66} & C_{66} & D_{16} & D_{26} & D_{66} & D_{66} & E_{16} & E_{26} & E_{66} & E_{66} \\ B_{16} & B_{26} & B_{66} & B_{66} & C_{16} & C_{26} & C_{66} & C_{66} & D_{16} & D_{26} & D_{66} & D_{66} & E_{16} & E_{26} & E_{66} & E_{66} \\ C_{11} & C_{12} & C_{16} & C_{16} & D_{11} & D_{12} & D_{16} & D_{16} & E_{11} & E_{12} & E_{16} & E_{16} & F_{11} & F_{12} & F_{16} & F_{16} \\ C_{12} & C_{22} & C_{26} & C_{26} & D_{12} & D_{22} & D_{26} & D_{26} & E_{12} & E_{22} & E_{26} & E_{26} & F_{12} & F_{22} & F_{26} & F_{26} \\ C_{16} & C_{26} & C_{66} & C_{66} & D_{16} & D_{26} & D_{66} & D_{66} & E_{16} & E_{26} & E_{66} & E_{66} & F_{16} & F_{26} & F_{66} & F_{66} \\ C_{16} & C_{26} & C_{66} & C_{66} & D_{16} & D_{26} & D_{66} & D_{66} & E_{16} & E_{26} & E_{66} & E_{66} & F_{16} & F_{26} & F_{66} & F_{66} \\ D_{11} & D_{12} & D_{16} & D_{16} & E_{11} & E_{12} & E_{16} & E_{16} & F_{11} & F_{12} & F_{16} & F_{16} & G_{11} & G_{12} & G_{16} & G_{16} \\ D_{12} & D_{22} & D_{26} & D_{26} & E_{12} & E_{22} & E_{26} & E_{26} & F_{12} & F_{22} & F_{26} & F_{26} & G_{12} & G_{22} & G_{26} & G_{26} \\ D_{16} & D_{26} & D_{66} & D_{66} & E_{16} & E_{26} & E_{66} & E_{66} & F_{16} & F_{26} & F_{66} & F_{66} & G_{16} & G_{26} & G_{66} & G_{66} \\ D_{16} & D_{26} & D_{66} & D_{66} & E_{16} & E_{26} & E_{66} & E_{66} & F_{16} & F_{26} & F_{66} & F_{66} & G_{16} & G_{26} & G_{66} & G_{66} \end{bmatrix} \begin{Bmatrix} \varepsilon_{0\alpha} \\ \varepsilon_{0\beta} \\ \varepsilon_{0\alpha\beta} \\ \varepsilon_{0\beta\alpha} \\ \varepsilon_{1\alpha} \\ \varepsilon_{1\beta} \\ \varepsilon_{1\alpha\beta} \\ \varepsilon_{1\beta\alpha} \\ \varepsilon_{2\alpha} \\ \varepsilon_{2\beta} \\ \varepsilon_{2\alpha\beta} \\ \varepsilon_{2\beta\alpha} \\ \varepsilon_{3\alpha} \\ \varepsilon_{3\beta} \\ \varepsilon_{3\alpha\beta} \\ \varepsilon_{3\beta\alpha} \end{Bmatrix} \tag{13}$$

The coefficients A_{mn} , B_{mn} , ... and G_{mn} are defined as follows:

$$(A_{mn}^i, B_{mn}^i, C_{mn}^i, D_{mn}^i, E_{mn}^i, F_{mn}^i, G_{mn}^i) = \sum_{k=1}^{N^i} \overline{Q}_{mn}^k \int_{z_{c_{k-1}}}^{z_{c_k}} (1, z_c, {z_c}^2, {z_c}^3, {z_c}^4, {z_c}^5, {z_c}^6) dz_c \tag{14}$$

3. Energy Termsand work done

The potential and kinetic energies of the entire system can be written as:

$$U_{Total} = U_t + U_c + U_b + U_E + U_{foundation} \tag{15}$$

$$T_{Total} = T_t + T_c + T_b$$

Where U_{Total} and T_{Total} stand for the system's potential and kinetic energies, respectively. U_E represents the potential energy corresponding to the virtual spring elements incorporated to simulate the boundary conditions, and $U_{foundation}$ is the potential energy of the elastic foundation. Each of these terms will be calculated in the following sections.

First, the potential energy of the main structural layers is introduced. For the top and bottom face sheets, we have:

$$U_i = \frac{1}{2}\int_\alpha\int_\beta \left\{ \begin{array}{l} N_\alpha^i \varepsilon_{0\alpha}^i + N_\beta^i \varepsilon_{0\beta}^i + N_{\alpha\beta}^i \varepsilon_{0\alpha\beta}^i + N_{\beta\alpha}^i \varepsilon_{0\beta\alpha}^i + M_\alpha^i \kappa_\alpha^i + M_\beta^i \kappa_\beta^i \\ + M_{\alpha\beta}^i \kappa_{\alpha\beta}^i + M_{\beta\alpha}^i \kappa_{\beta\alpha}^i + Q_\alpha^i \gamma_{0\alpha z}^i + Q_\beta^i \gamma_{0\beta z}^i \end{array} \right\} A_i B_i d\alpha d\beta \quad , \quad i = t, b \tag{16}$$

Similarly, the core's potential energy can be given by:

$$U_c = \frac{1}{2}\int_\alpha\int_\beta \left(\begin{array}{l} N_\alpha \varepsilon_{0\alpha} + M_{1\alpha} \varepsilon_{1\alpha} + M_{2\alpha} \varepsilon_{2\alpha} + M_{3\alpha} \varepsilon_{3\alpha} + N_\beta \varepsilon_{0\beta} + M_{1\beta} \varepsilon_{1\beta} + M_{2\beta} \varepsilon_{2\beta} + \\ M_{3\beta} \varepsilon_{3\beta} + R_z \varepsilon_{0z} + M_z \varepsilon_{1z} + Q_{\alpha z} \gamma_{0\alpha z} + M_{Q1\alpha z} \gamma_{1\alpha z} + M_{Q2\alpha z} \gamma_{2\alpha z} + M_{Q3\alpha z} \gamma_{3\alpha z} + \\ Q_{\beta z} \gamma_{0\beta z} + + M_{Q1\beta z} \gamma_{1\beta z} + M_{Q2\beta z} \gamma_{2\beta z} + M_{Q3\beta z} \gamma_{3\beta z} + N_{\alpha\beta} \gamma_{0\alpha\beta} + M_{1\alpha\beta} \gamma_{1\alpha\beta} + \\ M_{2\alpha\beta} \gamma_{2\alpha\beta} + M_{3\alpha\beta} \gamma_{3\alpha\beta} + N_{\beta\alpha} \gamma_{0\beta\alpha} + M_{1\beta\alpha} \gamma_{1\beta\alpha} + M_{2\beta\alpha} \gamma_{2\beta\alpha} + M_{3\beta\alpha} \gamma_{3\beta\alpha} \end{array} \right) A_c B_c d\alpha d\beta \tag{17}$$

Considering a Winkler-type elastic foundation, we have:

$$U_F = \frac{1}{2}\int_\alpha\int_\beta K_{foundation} w_b^{\,2} A_b B_b d\alpha d\beta \tag{18}$$

In which $K_{foundation}$ is the foundation stiffness. In addition, to model the boundary conditions, virtual springs are employed. Therefore, the potential energy associated with these springs must also be included in the total potential energy of the structure. Accordingly, we have:

$$U_E = U_{E1} + U_{E2} + U_{E3} + U_{E4} \tag{19}$$

Where U_{E1}, U_{E2}, U_{E3}, and U_{E4} represent the elastic potential energy due to springs located along the boundaries $\alpha = 0$, $\alpha = a$, $\beta = 0$, and $\beta = b$, respectively. These expressions are provided in detail in reference [26].

Meanwhile, the kinetic energy can be derived using the following expressions:

$$\begin{aligned} T_i &= \frac{1}{2}\int_\alpha\int_\beta \left\{ \bar{I}_0^i \left(\dot{u}_0^{i\,2} + \dot{v}_0^{i\,2} + \dot{w}_0^{i\,2} \right) + \bar{I}_1^i \left(\dot{\psi}_\alpha^{i\,2} + \dot{\psi}_\beta^{i\,2} \right) + \bar{I}_2^i \left(\dot{u}_0^i \dot{\psi}_\alpha^i + \dot{v}_0^i \dot{\psi}_\beta^i \right) \right\} A_i B_i d\alpha d\beta \\ T_c &= \frac{1}{2}\int_\alpha\int_\beta \left\{ \begin{array}{l} \bar{I}_0^c \left(\dot{u}_0^{\,2} + \dot{v}_0^{\,2} + \dot{w}_0^{\,2} \right) + 2\bar{I}_1^c \left(\dot{u}_0 \dot{u}_1 + \dot{v}_0 \dot{v}_1 + \dot{w}_0 \dot{w}_1 \right) \\ + \bar{I}_2^c \left(2\dot{u}_0 \dot{u}_2 + \dot{u}_1^{\,2} + 2\dot{v}_0 \dot{v}_2 + \dot{v}_1^{\,2} + 2\dot{w}_0 \dot{w}_2 + \dot{w}_1^{\,2} \right) + \\ 2\bar{I}_3^c \left(\dot{u}_0 \dot{u}_3 + \dot{u}_1 \dot{u}_2 + \dot{v}_0 \dot{v}_3 + \dot{v}_1 \dot{v}_2 + \dot{w}_1 \dot{w}_2 \right) + \bar{I}_4^c \left(2\dot{u}_1 \dot{u}_3 + \dot{u}_2^{\,2} + 2\dot{v}_1 \dot{v}_3 + \dot{v}_2^{\,2} + \dot{w}_2^{\,2} \right) \\ + 2\bar{I}_5^c \left(\dot{u}_2 \dot{u}_3 + \dot{v}_2 \dot{v}_3 \right) + \bar{I}_6^c \left(\dot{u}_3^{\,2} + \dot{v}_3^{\,2} \right) \end{array} \right\} A_c B_c d\alpha d\beta \end{aligned} \tag{20}$$

Where $\bar{I}_j^i$ (with $i = t, b, c$ and $j = 0, 1, ..., 6$) are the inertia coefficients, formulated as:

$$\left[\bar{I}_0^i, \bar{I}_1^i, \bar{I}_2^i, \bar{I}_3^i\right] = \int_{\frac{-h_i}{2}}^{\frac{h_i}{2}} \rho_i \left[1, z_i, {z_i}^2, {z_i}^3\right]\left(1+\frac{z_i}{R^i}\right)\left(1+\frac{z_i}{R^i}\right)dz_i$$
$$\left[\bar{I}_0^c, \bar{I}_1^c, \bar{I}_2^c, \bar{I}_3^c, \bar{I}_4^c, \bar{I}_5^c, \bar{I}_6^c\right] = \int_{\frac{-h_c}{2}}^{\frac{h_c}{2}} \rho_c \left[1, z_c, {z_c}^2, {z_c}^3, {z_c}^4, {z_c}^5, {z_c}^6\right]\left(1+\frac{z_c}{R^c}\right)\left(1+\frac{z_c}{R^c}\right)dz_c \quad (21)$$

Where ρ_i (with $i = t, b, c$) denotes the density values for each layer. Finally, the work done by the external force is expressed as:

$$W_F = \int_\alpha \int_\beta F(t) w_t \left(1+\frac{z_t}{R^t}\right)\left(1+\frac{z_t}{R^t}\right) AB d\alpha d\beta \quad (22)$$

Where w_t refers to the transverse displacement (deflection) of the top layer, as previously mentioned, chosen because the impact load is exerted on the top of the structure. By considering the perfect bonding conditions between the main layers of the structure, a reduction in the number of variables can be achieved. Therefore, the compatibility conditions can be expressed as follows:

$$\begin{aligned}
&u_c\left(z_c = -\frac{h_c}{2}\right) = u_t\left(z_t = \frac{h_t}{2}\right) && u_c\left(z_c = \frac{h_c}{2}\right) = u_b\left(z_b = -\frac{h_b}{2}\right)\\
&v_c\left(z_c = -\frac{h_c}{2}\right) = v_t\left(z_t = \frac{h_t}{2}\right) && v_c\left(z_c = \frac{h_c}{2}\right) = v_b\left(z_b = -\frac{h_b}{2}\right)\\
&w_c\left(z_c = -\frac{h_c}{2}\right) = w_t\left(z_t = \frac{h_t}{2}\right) && w_c\left(z_c = \frac{h_c}{2}\right) = w_b\left(z_b = -\frac{h_b}{2}\right)
\end{aligned} \quad (23)$$

Using the displacement fields of the main layers, we have:

$$\begin{aligned}
u_2 &= \frac{2\left(u_0^b + u_0^t\right) - h_b\psi_\alpha^b + h_t\psi_\alpha^t - 4u_0}{{h_c}^2}\\
u_3 &= \frac{4\left(u_0^b - u_0^t\right) - 2(h_b\psi_\alpha^b + h_t\psi_\alpha^t) - 4h_c u_1}{{h_c}^3}\\
v_2 &= \frac{4\left(v_0^b + v_0^t\right) - h_b\psi_\beta^b + h_t\psi_\beta^t - 4h_c v_0}{{h_c}^2}\\
v_3 &= \frac{4\left(v_0^b - v_0^t\right) - 2(h_b\psi_\beta^b + h_t\psi_\beta^t) - 4h_c v_1}{{h_c}^3}\\
w_1 &= \frac{w_0^b - w_0^t}{h_c}\\
w_2 &= \frac{2(w_0^b + w_0^t - 2w_0)}{{h_c}^2}
\end{aligned} \quad (24)$$

Thus, the problem involves a total of 15 variables.

4. Finite element method

Here, to obtain the discrete equations of motion, the finite element method is applied. To achieve this, a nine-node high-order element is utilised, with each node having 15 degrees of freedom that align with the problem's variable count. Therefore, the nodal degree of freedom vector for each element can be defined as follows:

$$\{\delta\} = \{\{d_1\},\{d_2\},\{d_3\},\{d_4\},\{d_5\},\{d_6\},\{d_7\},\{d_8\},\{d_9\}\}^T \tag{25}$$

Where $\{\delta\}$ denotes the degree of freedom vector for the element and $\{d_i\}$ denotes the DOF (Degrees of Freedom) vector for each node, expressed as:

$$\{d_i\} = \left\{u_{0i}^t, \psi_{\alpha i}^t, v_{0i}^t, \psi_{\beta i}^t, w_{0i}^t, u_{0i}^b, \psi_{\alpha i}^b, v_{0i}^b, \psi_{\beta i}^b, w_{0i}^b, u_{0i}, u_{1i}, v_{0i}, v_{1i}, w_{0i}\right\}^T \tag{26}$$

By employing interpolation functions, the variables can be expressed as:

$$\begin{aligned}
&u_0^t = \left[N_{u_0^t}\right]\{\delta\} \quad && \psi_\alpha^t = \left[N_{\psi_\alpha^t}\right]\{\delta\} \quad && v_0^t = \left[N_{v_0^t}\right]\{\delta\} \quad && \psi_\beta^t = \left[N_{\psi_\beta^t}\right]\{\delta\} \quad && w_0^t = \left[N_{w_0^t}\right]\{\delta\} \\
&u_0^b = \left[N_{u_0^b}\right]\{\delta\} && \psi_\alpha^b = \left[N_{\psi_\alpha^b}\right]\{\delta\} && v_0^b = \left[N_{v_0^b}\right]\{\delta\} && \psi_\beta^b = \left[N_{\psi_\beta^b}\right]\{\delta\} && w_0^b = \left[N_{w_0^b}\right]\{\delta\} \\
&u_0 = \left[N_{u_0}\right]\{\delta\} && u_1 = \left[N_{u_1}\right]\{\delta\} && v_0 = \left[N_{v_0}\right]\{\delta\} && v_1 = \left[N_{v_1}\right]\{\delta\} && w_0 = \left[N_{w_0}\right]\{\delta\}
\end{aligned} \tag{27}$$

The Lagrange interpolation functions are used in the above variables. By considering the above relations and substituting them into the expressions for the kinetic energy, the potential energy, and the work done by the external force, the mass matrix, stiffness matrix, and corresponding force vector for each element can be obtained, respectively:

$$\begin{aligned}
T &= \frac{1}{2}\{\dot{\delta}\}^T [M_e]\{\dot{\delta}\} \\
U &= \frac{1}{2}\{\delta\}^T [K_e]\{\delta\} \\
W_F &= \{\delta\}^T [F_e]
\end{aligned} \tag{28}$$

Following assembly, the governing equations of motion are derived as:

$$\mathbf{M\ddot{d} + Kd = F}(t) \tag{29}$$

Where $\mathbf{d}(t)$ represents the total nodal displacement vector, $\ddot{\mathbf{d}}(t)$ is the total nodal acceleration vector, and $\mathbf{F}(t)$ denotes the external excitation force vector caused by the impact load.

4.1. Free vibration analysis

By setting $\mathbf{F}(t) = \mathbf{0}$, assuming $\mathbf{d} = \Phi \mathbf{e}^{i\omega t}$, and substituting it into Equation (29), while neglecting the term $\mathbf{e}^{i\omega t}$, we obtain:

$$(\mathbf{K} - \omega^2 \mathbf{M})\Phi = \mathbf{0} \tag{30}$$

Where ω and Φ denote the eigenfrequencies and their associated mode shapes, respectively.

4.2. Forced vibration analysis

This section focuses on the dynamic response of the structure under impact loads is investigated. To this end, Rayleigh damping is considered. Accordingly, the governing equations of motion for the structure can be expressed as follows:

$$\mathbf{M}\ddot{\mathbf{d}}(t) + \mathbf{C}\dot{\mathbf{d}}(t) + \mathbf{K}\mathbf{d}(t) = \mathbf{F}(t) \tag{31}$$

Where $\mathbf{M}$, $\mathbf{K}$, and $\mathbf{C}$ denote the global mass, stiffness, and damping matrices, respectively; $\mathbf{F}(t)$ is the time-dependent external force vector. As mentioned before, $\mathbf{d}(t)$, $\dot{\mathbf{d}}(t)$, and $\ddot{\mathbf{d}}(t)$ represent the displacement, velocity, and acceleration vectors at time t, respectively. To account for both material and structural damping proportionally, Rayleigh damping is employed, where the damping matrix is defined as:

$$\mathbf{C} = \eta_1\mathbf{M} + \eta_2\mathbf{K} \tag{32}$$

In Which η_1 and η_2 are the Rayleigh damping coefficients, which can be calculated using the following relations:

$$\begin{bmatrix} 1 & \omega_1^{\,2} \\ 1 & \omega_2^{\,2} \end{bmatrix} \begin{Bmatrix} \eta_1 \\ \eta_2 \end{Bmatrix} = 2\zeta \begin{Bmatrix} \omega_1 \\ \omega_2 \end{Bmatrix} \tag{33}$$

Where ω_1 and ω_2 are the fundamental and second natural frequencies, in sequence, and ζ denotes the damping ratio of the system. A damping ratio of $\xi = 0.02$ is assumed for all modes [28].

The reaction of the system is determined by solving equation (31). To accomplish this, the Newmark method is utilised. This method is a numerical time integration technique derived from the finite difference approach. Using this method, the system's behaviour over the time period $\overline{T}$. Consequently, the entire duration of the analysis is partitioned into n smaller time increments as follows:

$$\Delta t = \frac{\overline{T}}{n} \tag{34}$$

Therefore:

$$t_n = n\Delta t \quad , \quad n = 1,2,3,...,n \tag{35}$$

According to this method, the system response at time t_{n+1} is determined by solving the following equation:

$$\left[\overline{K}\right]_{n+1} \{\delta\}_{n+1} = \left\{\overline{F}\right\}_{n+1} \tag{36}$$

In this expression:

$$\begin{aligned} \left[\overline{K}\right]_{n+1} &= \left[K\right]_{n+1} + a_0\left[M\right]_{n+1} + a_1\left[C\right]_{n+1} \\ \left[\overline{F}\right]_{n+1} &= \left[F\right]_{n+1} + \left[M\right]_{n+1}\left(a_0\delta_n + a_2\dot{\delta}_n + a_3\ddot{\delta}_n\right) + \left[C\right]_{n+1}\left(a_1\delta_n + a_4\dot{\delta}_n + a_5\ddot{\delta}_n\right) \end{aligned} \tag{37}$$

After computing δ_{n+1} from equation (36), using the relations below, the velocity and acceleration of the system can be obtained:

$$\begin{cases} \ddot{\delta}_{n+1} = a_0(\delta_{n+1} - \delta_n) - a_2\dot{\delta}_n - a_3\ddot{\delta}_n \\ \dot{\delta}_{n+1} = \dot{\delta}_n + a_6\ddot{\delta}_n + a_7\ddot{\delta}_n \end{cases} \tag{38}$$

In which the coefficients a_0, a_1, …, and a_7 are defined as follows:

$$a_0 = \frac{1}{\overline{\beta}\Delta t^2} \qquad a_1 = \frac{\overline{\alpha}}{\overline{\beta}\Delta t} \qquad a_2 = \frac{1}{\overline{\beta}\Delta t} \qquad a_3 = \frac{1}{2\overline{\beta}} - 1$$
$$a_4 = \frac{\overline{\alpha}}{\overline{\beta}} - 1 \qquad a_5 = \frac{\Delta t}{2}\left(\frac{\overline{\alpha}}{\overline{\beta}} - 2\right) \qquad a_6 = \left(1 - \overline{\alpha}\right)\Delta t \qquad a_7 = \overline{\alpha}\Delta t \tag{39}$$

In which $\overline{\alpha}$ and $\overline{\beta}$ are the parameters used in the Newmark Method.

5. Results and discussion

5.1. Free Vibration Analysis

This section presents the numerical results derived from the proposed formulation. To this end, a spherical sandwich panel is considered, in which the face sheets are composed of multilayer composite materials, and the core is made of a flexible foam. The material properties of the face sheets and the core are provided in Table 1. Throughout the study, unless otherwise stated, it is assumed the core is made of material M1, and the face sheets are made of material M2, and have the following geometric ratios: length-to-width $a/b = 1$, length-to-thickness $a/h = 10$, $h_c/h_f = 10$, and curvature radius-to-length $R/a = 1$. The top and bottom face sheets are assumed to be composed of a symmetric laminated composite with a fiber orientation of $[0/90/0]$. Furthermore, a notation is adopted to represent the kind of boundary conditions. For example, the boundary condition denoted as CSCF refers to a configuration where the edges $\alpha = 0$, $\beta = 0$, $\alpha = a$, and $\beta = b$ are clamped, simply supported, clamped, and free, respectively. It should be mentioned that the nondimensional natural frequency parameter is defined as $\Omega = \omega a^2 \sqrt{(\rho_c / E_c)}/h$.

Table 1. Material properties of the face sheets and core

Property	Unit	M1	M2	M3	M4	M5
E_1	GPa	0.1036	24.51	0.00689	131	128
E_2	GPa	0.1036	7.77	0.00689	10.34	11
E_3	GPa	0.1036	7.77	0.00689	10.34	11
G_{12}	GPa	0.05	3.34	0.00345	6.895	4.48
G_{23}	GPa	0.05	1.34	0.00345	6.895	4.48
G_{13}	GPa	0.05	3.34	0.00345	6.205	1.53
υ_{12}	-	0.33	0.078	0	0.22	0.25
υ_{13}	-	0.33	0.49	0	0.22	0.25
υ_{23}	-	0.33	0.078	0	0.49	
ρ	kg/m^3	130	1800	94.195	1627	1500

To determine an appropriate mesh size that yields sufficiently accurate results, a convergence study was conducted based on the first six fundamental dimensionless natural frequencies of the structure. The corresponding results for mesh configurations of 4×4, 6×6, 8×8, 10×10, and 12×12 are presented in Table 2. Based on these findings, it can be concluded that the 10×10 mesh provides a satisfactory balance between solution accuracy and computational cost. Therefore, this mesh configuration is adopted for all subsequent analyses presented in this study. The undeformed shape of spherical panel and the first 5 mode shapes are shown in following Figure 2.

Table 2. Study of Convergence for the First Six non-Dimensional Frequencies

	Natural Frequencies ($\Omega = \omega a^2 \sqrt{(\rho_c / E_c)} / h$)					
$m \times n$	Ω_1	Ω_2	Ω_3	Ω_4	Ω_5	Ω_6
4×4	22.5138	32.067	32.5002	37.3683	39.1626	39.1803
6×6	22.8968	32.109	32.6468	37.3287	40.0673	40.0772
8×8	23.1374	32.2342	32.8178	37.446	40.5945	40.6005
10×10	23.2987	32.3316	32.9431	37.5457	40.9371	40.9409
12×12	23.2987	32.3316	32.9431	37.5457	40.9371	40.9409

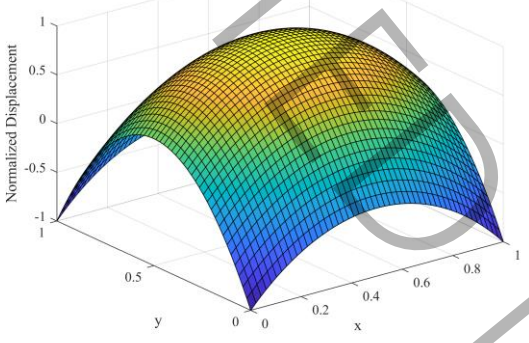

(a)

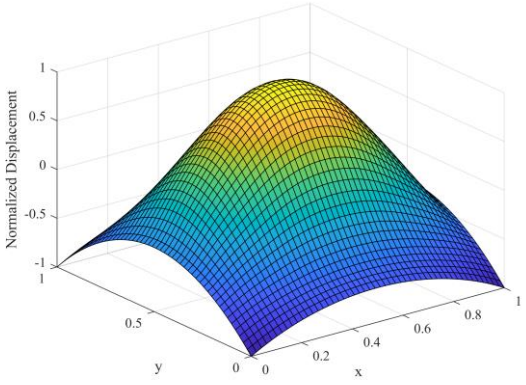

(b)

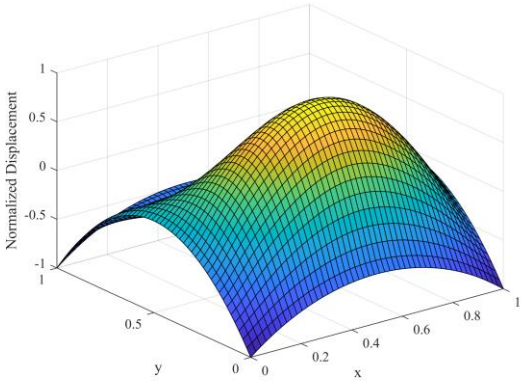

(c)

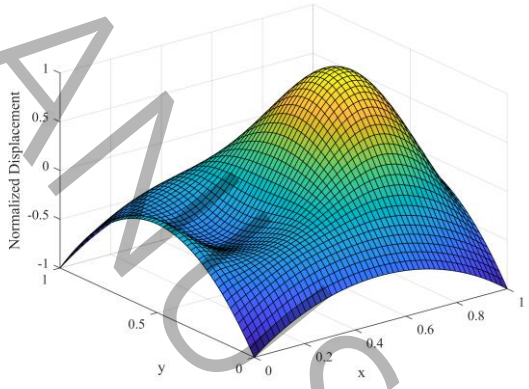

(d)

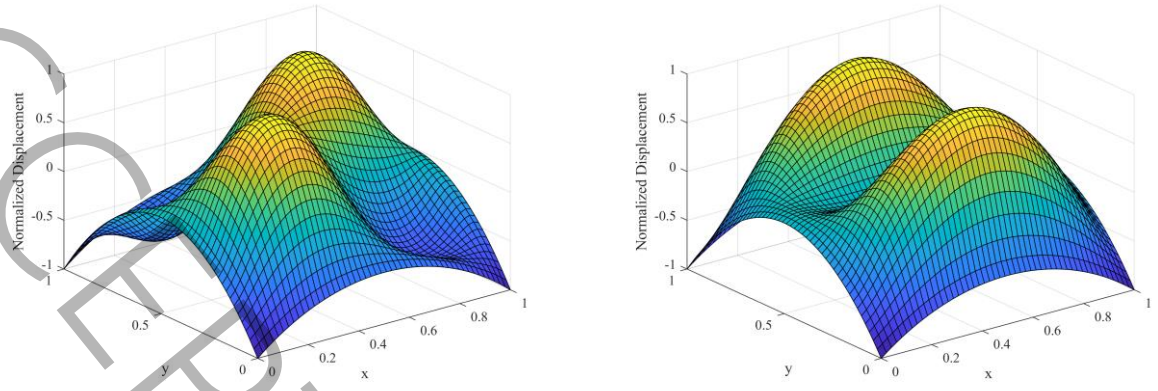

(e) (F)

Figure 2. (a) undeformed, and first five mode shapes corresponding to modes (b) (1,1), (c) (1,2), (d) (2,1), (e) (2,2), and (f) (3,1)

Having determined the appropriate mesh configuration, it is necessary to verify the validity of the proposed formulation. For this purpose, a comparison is conducted among the present findings and reported ones in reputable references. First, to validate the free vibration response, the dimensionless fundamental frequencies of a spherical shell are compared in Table 3, where other studies have employed HSAPT [29], and Equivalent Single Layer Theory (ESLT) [30]. Table 3 demonstrates a close agreement among the results, confirming the reliability of both the proposed formulation and the solution technique used in this study. For the purposes of validation, material M3 was designated for the core, whereas material M4 was allocated to the face sheets. Furthermore, the stacking sequence for both the top and bottom face sheets is specified as follows. $[0/90]$.

Table 3. Validation of present results and available results in the literature ($[0/90/core/0/90]$, M3 and M4, SSSS boundary condition)

a/h	R/a	Present	HSAPT [29]	ESLT [30]
100	1	123.47	123.56	123.57
	2	65.74	65.86	66.33
	3	45.14	45.24	46.11
	5	28.85	28.95	30.45
10	1	12.15	12.29	12.94
	2	6.64	6.71	8
	3	4.68	4.73	6.52
	5	3.19	3.22	5.58

In the next step, the forced vibration response is validated. For this purpose, the case study reported by Nayak et al. [31] is considered: a simply supported square sandwich plate, consisting of laminated composite face sheets and a soft core. Material properties M1 and M5 are adopted for the core and the face sheets, respectively. The length-to-thickness ratio is set to a/h=10, and the ratio of the total face-sheet thickness to the overall plate thickness is taken as $h_f/h=0.1$, where h_f denotes the combined thickness of both face sheets.

The lamination is defined as $[0/90/0/90/core/90/0/90/0]$ and a transverse load of the form $q(x,y,t) = q_0 F(t)\sin(\frac{\pi x}{a})\sin(\frac{\pi y}{b})$ is applied on the top face sheet. The time-dependent load function $F(t)$ is defined as follows: $F(t) = 0$ for $t > t_1$, while for $t \le t_1$, $F(t) = 1$ for step loading, $F(t) = \sin(\frac{\pi t}{t_1})$ for sinusoidal loading, and $F(t) = e^{-\gamma t_1}$ for blast loading. The parameters used are $\gamma = 330\text{s}^{-1}$, $t_1 = 0.006\text{s}$, and $q_0 = 68.9476\text{MPa}$. A validation of the proposed model is carried out by contrasting its computed central deflection for the sandwich plate against the benchmark data provided by Nayak et al. [31], with the outcomes illustrated in Figure 3. It should be noted that the plate length was not specified in Ref. [31], and the reported central deflection was given in dimensional form; therefore, the corresponding normalization was carried out to ensure a consistent comparison.

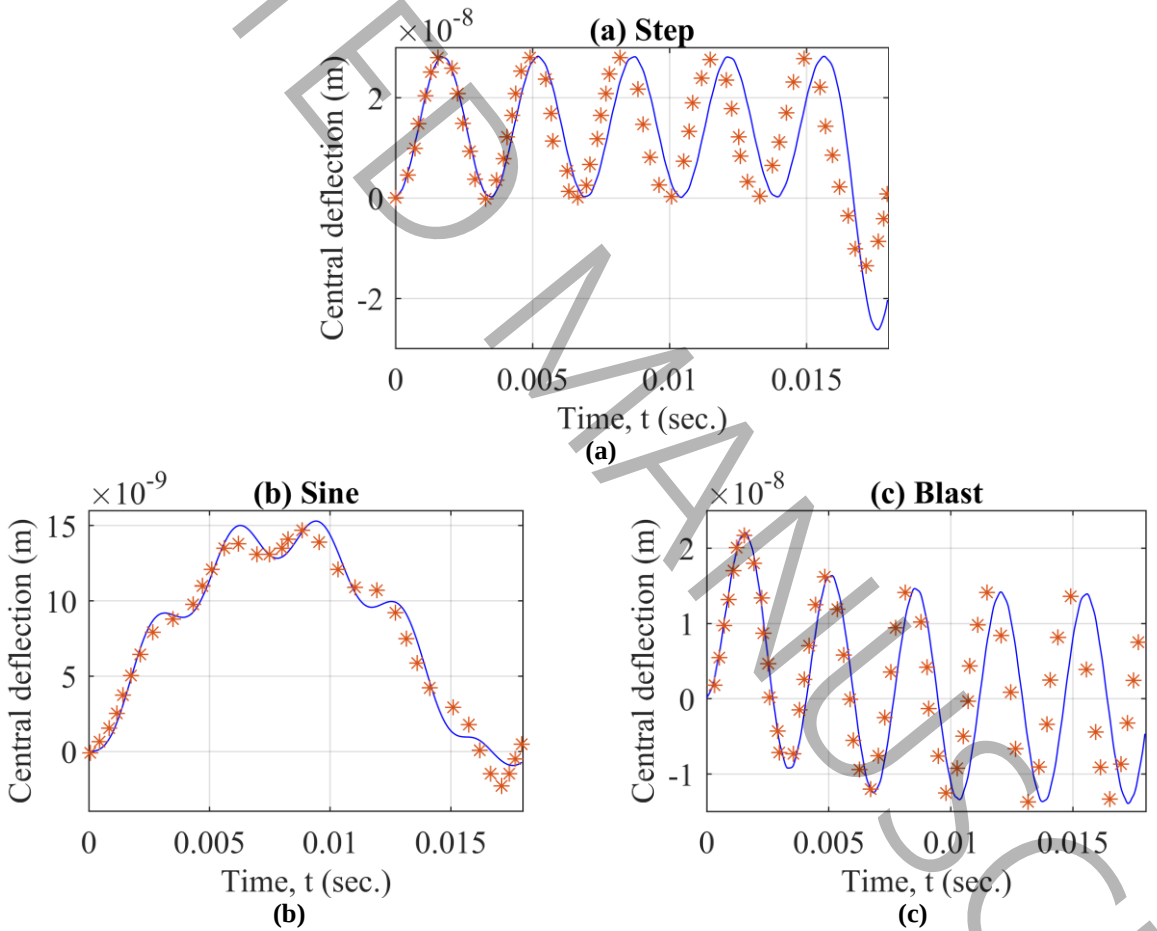

Figure 3. Central deflection of sandwich plate subjected to impulsive loads, (a) step loading, (b) sinusoidal loading, and (c) exponential blast loading (continuous blue line: present formulation, red stars: reference [31])

This section investigates how various parameters influence the vibrational behavior of the system. As a first step, the analysis focuses on assessing the impact of different boundary conditions and the presence of an elastic foundation on

the natural frequencies. The results are presented for several boundary conditions, including SSSS, CCCC, CFFF, CSCF, CFCF, and FFFF. Moreover, comparisons are made between the cases without an elastic foundation and with elastic foundations of varying stiffness values. As expected, the highest natural frequency corresponds to the fully clamped (CCCC) boundary condition, while the lowest frequency is observed under the FFFF condition. Additionally, an increase in the stiffness of the elastic foundation leads to a rise in the natural frequency of the system. The results are reported in Table 4.

Table 4. Non-dimensional fundamental natural frequencies for different boundary conditions with varying elastic foundation stiffness values

	Boundary Condition					
	CCCC	CSCF	CFCF	SSSS	CFFF	FFFF
$K_f = 0$ N/m	36.3949	26.5971	25.9011	23.2987	4.8625	3.3960
$K_f = 100$ N/m	36.3987	26.6019	25.9060	23.3041	4.8855	3.4319
$K_f = 1000$ N/m	36.4323	26.6452	25.9499	23.3532	5.0883	3.7397
$K_f = 10000$ N/m	36.7661	27.0726	26.3840	23.8374	6.7839	5.0207

The fundamental non-dimensional natural frequencies corresponding to various core-to-face sheet thickness ratios (h_c/h_f), along with different length-to-width ratios (a/b), length-to-thickness ratios (a/h), and curvature radius-to-length ratios (R/a), are presented in Table 5 to Table 7, respectively. The results indicate that increasing the length-to-width ratio (a/b) or the length-to-thickness ratio (a/h) results in higher natural frequencies. Moreover, as the ratio of curvature radius to length (R/a) increases, the natural frequencies tend to decrease.

Table 5. Effect of the length-to-width ratio (a/b) and core-to-face thickness ratio (h_c/h_f)
($R/a = 1$, $a/h = 10$, SSSS boundary condition, $[0/90/0/core/0/90/0]$)

h_c/h_f	$a/b = 1$	$a/b = 1.5$	$a/b = 2$	$a/b = 2.5$	$a/b = 3$
1	25.2870	28.6009	32.9801	37.9479	43.5125
5	24.6291	28.2250	32.7259	37.4603	42.2907
10	23.9959	28.1877	33.4874	39.1011	44.8001
20	22.7212	27.5933	33.9433	40.8268	47.8894
30	21.5978	26.7604	33.6642	41.2921	49.2001

Table 6. Effect of length-to-thickness ratio (a/h) and core-to-face thickness ratio (h_c/h_f)
($R/a = 1$, $a/b = 1$, SSSS boundary condition, $[0/90/0/core/0/90/0]$)

h_c/h_f	$a/h = 10$	$a/h = 30$	$a/h = 50$	$a/h = 75$	$a/h = 100$
1	25.2870	73.0375	120.7695	180.6740	237.5663
5	24.6291	68.5831	113.5801	170.1712	226.9390
10	23.9959	66.3762	107.9273	161.2682	214.8019
20	22.72118	60.7559	99.2493	147.8597	196.2141
30	21.5978	56.6517	92.4676	137.4177	183.1965

Table 7. Influence of the radius-to-length ratio (R/a) and core-to-face thickness ratio (h_c/h_f)
($a/b = 1$, $a/h = 10$, SSSS boundary condition, $[0/90/0/core/0/90/0]$)

h_c/h_f	$R/a = 1$	$R/a = 2$	$R/a = 5$	$R/a = 10$	$R/a = 25$

1	25.2870	16.1162	11.9662	11.2318	11.0166
5	24.6291	16.4917	13.0426	12.4600	12.2914
10	23.9959	17.0708	14.3303	13.8861	13.7588
20	22.72118	17.1917	15.1415	14.8199	14.7283
30	21.5978	16.8169	15.0955	14.8289	14.7532

5.2. Forced vibration analysis

This section examines the dynamic behaviour of the structure subjected to various impact loadings is investigated. The applied impact forces include different pulse shapes such as half-sine, rectangular, triangular, exponential, Gaussian, and full-sine pulses. In the results presented in the following tables and figures, the intensity of the impact force is taken as $F_0 = 10^5\,\mathrm{N}$. The Newmark parameters are chosen as $\overline{\alpha} = 0.25$, and $\overline{\beta} = 0.5$. The impact force acts over a duration of $0.01\mathrm{s}$, and the time history of the system's response is plotted over a total period of $0.1\mathrm{s}$. It should be mentioned that the pulse is applied at the central point of the top layer ($\alpha = a/2$, $\beta = b/2$). The profiles of the different impact functions are illustrated in Figure 4.

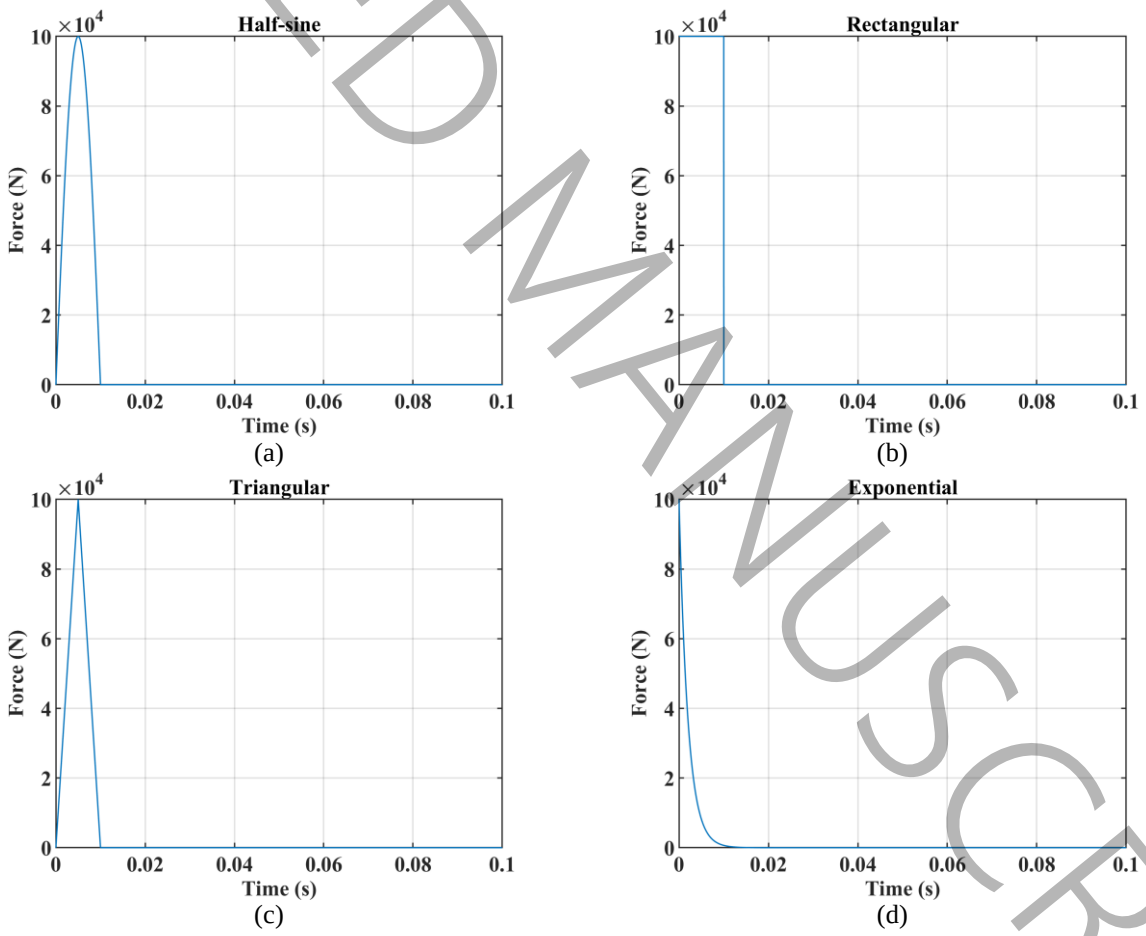

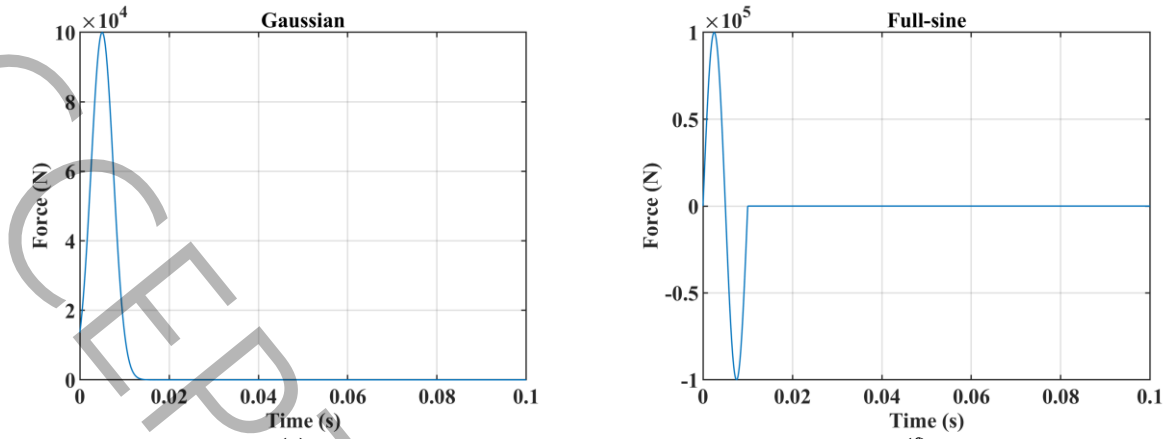

(e) (f)

Figure 4. Illustration of different impact load functions, (a) Half-Sine, (b) Rectangular, (c) Triangular, (d) Exponential, (e) Gaussian, and (f) Full-Sine

Figure 5 through Figure 7 illustrate the investigation of how various impact functions influence the structural response. The time histories of displacement, velocity, and acceleration are plotted for a structure with CFCF boundary conditions, in the absence of an elastic foundation, under various types of impact loading. For better comparison, the maximum values of displacement, velocity, and acceleration for each pulse shape are reported in Table 8 to Table 10.

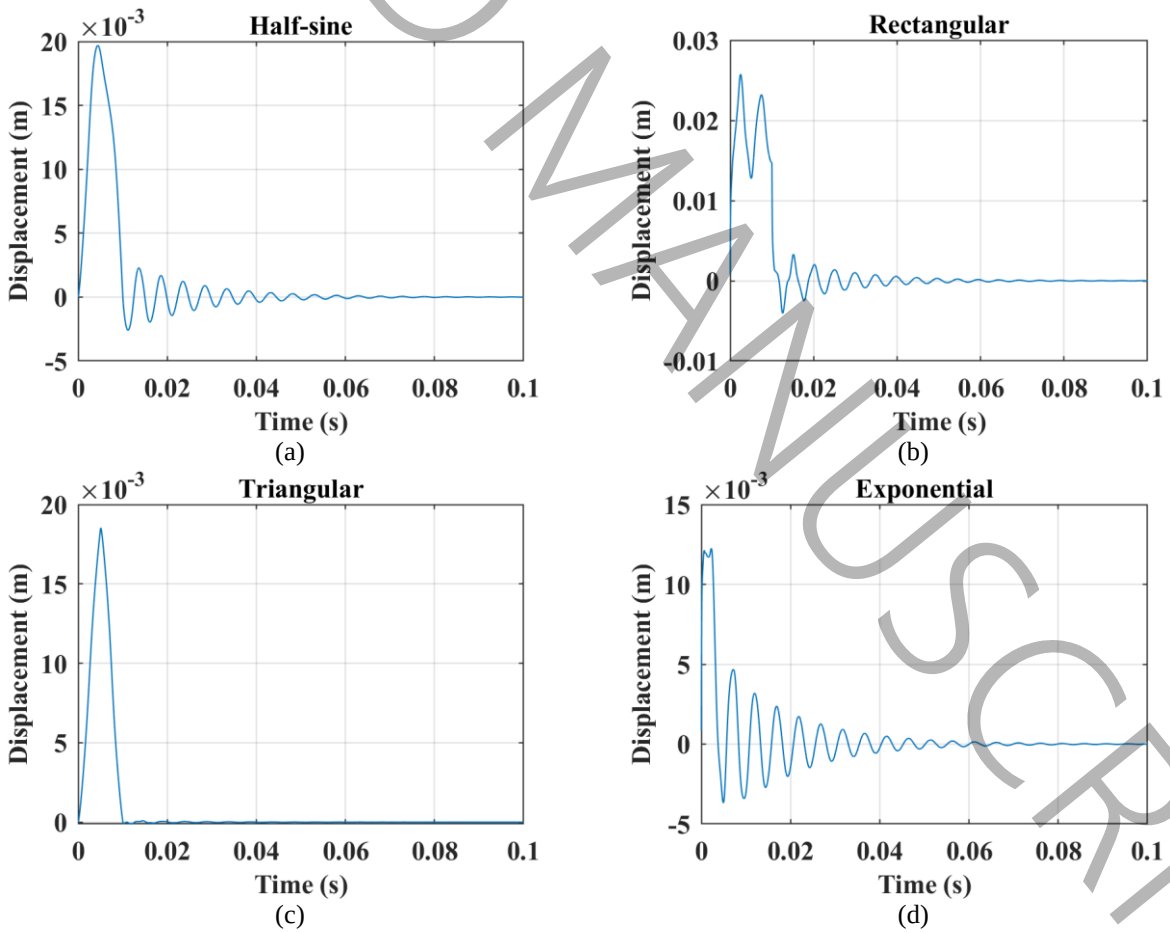

(a) (b)

(c) (d)

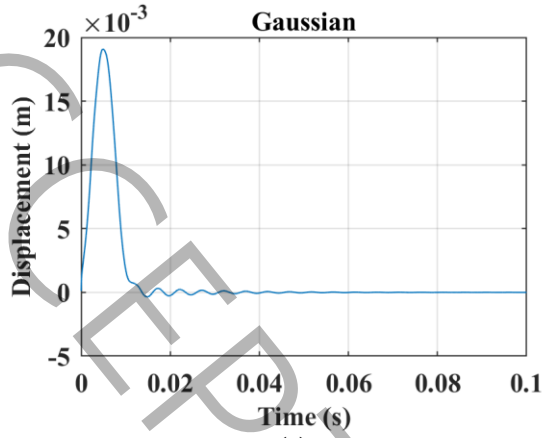

(e)

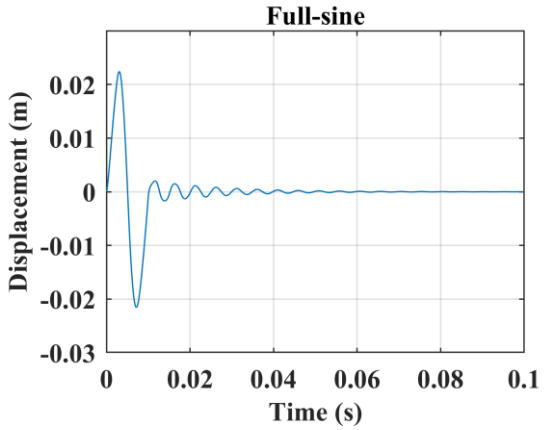

(f)

Figure 5. Displacement for the CFCF boundary condition without an elastic foundation under different impact load functions, (a) Half-Sine, (b) Rectangular, (c) Triangular, (d) Exponential, (e) Gaussian, and (f) Full-Sine

Table 8. Maximum values of displacement response for various pulse shapes

Impulse Type	Half-sine	Rectangular	Triangular	Exponential	Gaussian	Full-sine
Displacement (m)	0.0197	0.0258	0.0185	0.0123	0.0191	0.0224

Figure 5 and Table 8 show that the rectangular impulse load provides the most abrupt displacement profile due to its instantaneous loading nature, reaching maximum deflection quickly. In contrast, Gaussian and exponential loads yield smoother and more gradual displacement curves because they dissipate energy over long durations of time. Half-sine and triangular loads exhibit intermediate behaviour, while the full-sine load shows symmetrical oscillatory displacement profiles. The magnitude of displacement is directly proportional to the loading rate, with abrupt loads causing greater peak deflections.

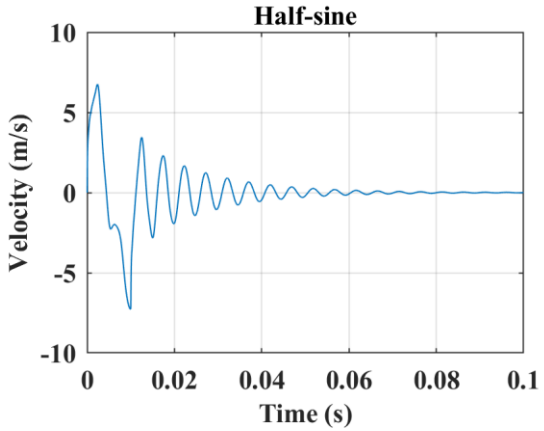

(a)

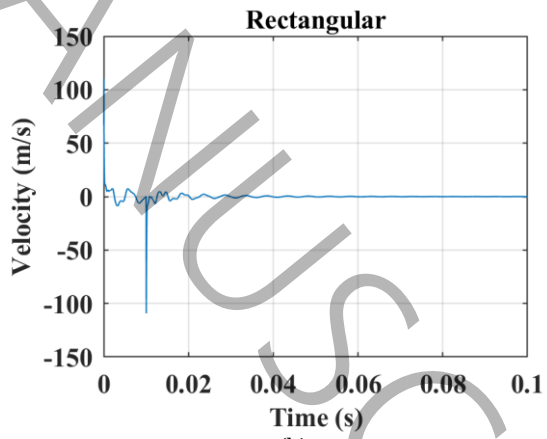

(b)

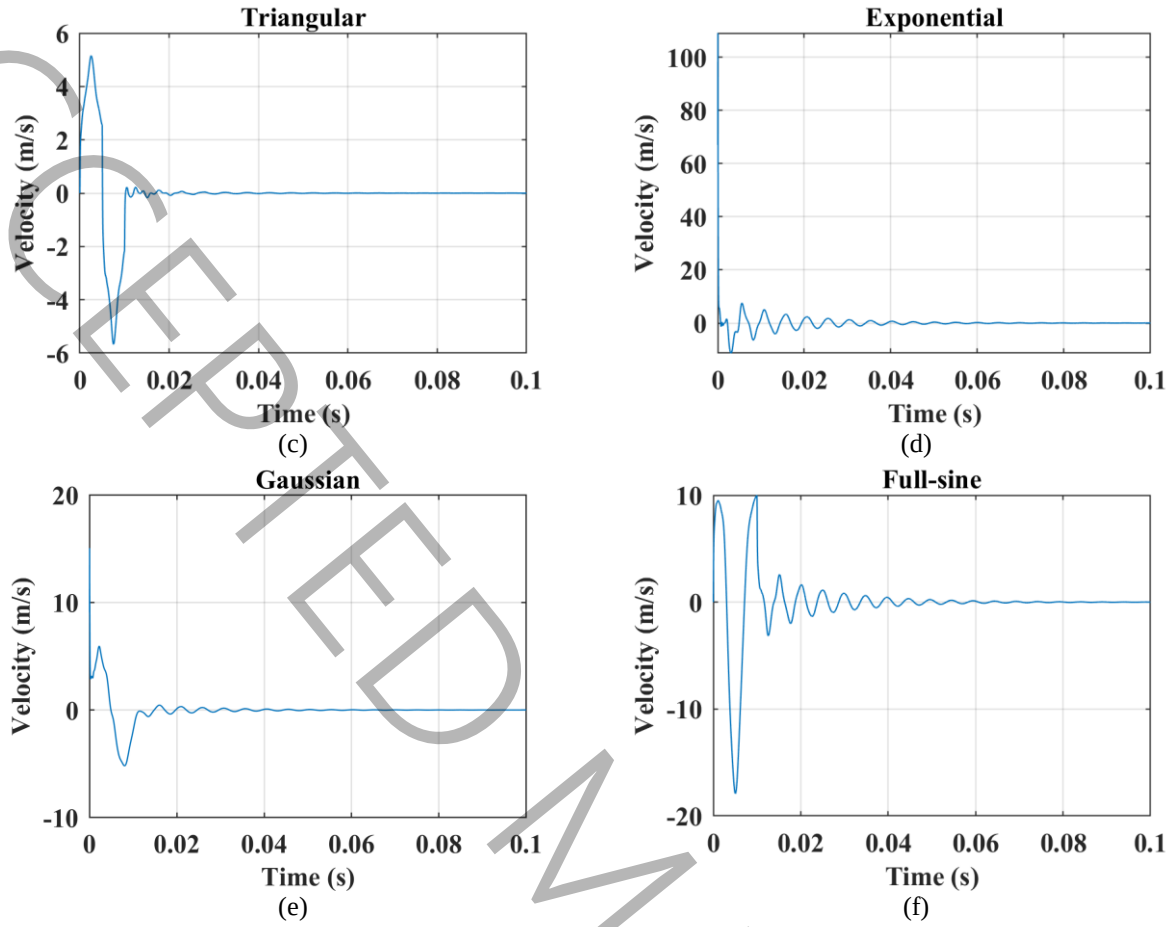

Figure 6. Velocity for the CFCF boundary condition without an elastic foundation under different impact load functions, (a) Half-Sine, (b) Rectangular, (c) Triangular, (d) Exponential, (e) Gaussian, and (f) Full-Sine

Table 9. Maximum values of velocity response for various pulse shapes

Impulse Type	Half-sine	Rectangular	Triangular	Exponential	Gaussian	Full-sine
Velocity (m/s)	6.7495	109.8773	5.1525	109.0453	15.0529	9.9923

Figure 6 and Table 9 show that rectangular and exponential loadings produce dangerous velocity spikes which can generate structural damage, whereas Gaussian, triangular, full-sine, and half-sine loadings produce the least varying velocity. Exponential loads have characteristic velocity decay, and sinusoidal types produce oscillatory velocity variations. The velocity time history shows the rate of transfer of kinetic energy to the structure, where more severe loading is represented by steeper velocity plots.

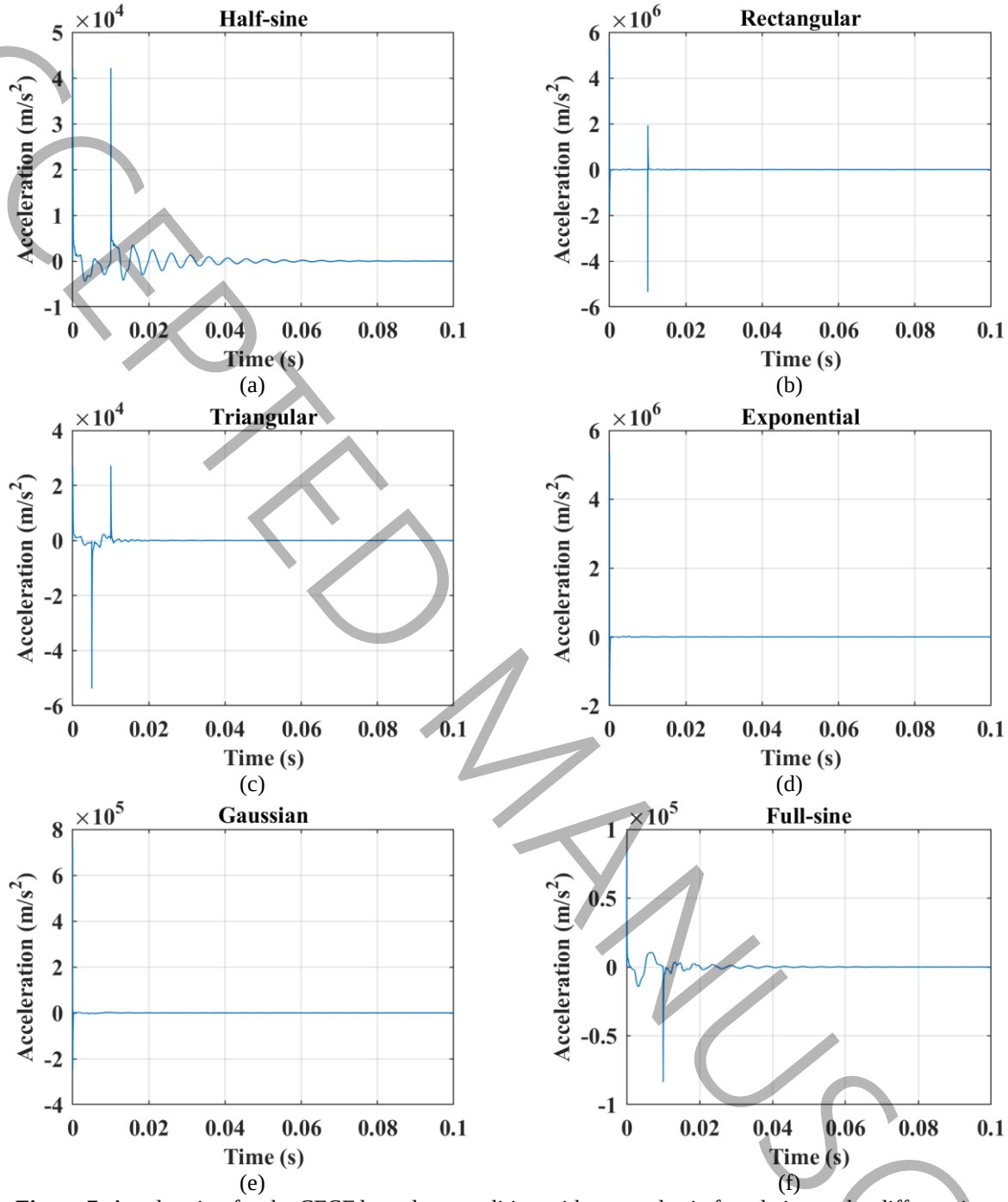

Figure 7. Acceleration for the CFCF boundary condition without an elastic foundation under different impact load functions, (a) Half-Sine, (b) Rectangular, (c) Triangular, (d) Exponential, (e) Gaussian, and (f) Full-Sine

Table 10. Maximum values of acceleration response for various pulse shapes

Impulse Type	Half-sine	Rectangular	Triangular	Exponential	Gaussian	Full-sine
Acceleration (m/s^2)	42205	5358100	27184	5358100	725140	84162

The most critical conclusions arise in acceleration analysis, and from Figure 7, it can be concluded that rectangular impulses yield extreme instant accelerations that may exceed design criteria, while Gaussian, triangular, half-sine, and full-sine loadings give smooth, low-level acceleration profiles. Triangular loads give linear acceleration changes, and exponential loads give rapid initial acceleration followed by steady decay. The findings reveal that the dynamic behavior of the structural system is highly influenced by the profile of the applied impulse load. The rectangular and exponential impulses of all loading types considered produce the most severe responses, yielding extremely large acceleration spikes of the order of $10^6 \mathrm{m/s^2}$, and the highest velocity peaks, due to their abrupt, step-like application that excites high-frequency structural modes. In contrast, the smoother impulses represented by the half-sine, triangular, Gaussian, and full-sine functions yield much lower peak responses and a typical damped oscillatory behavior, and characterize a more gradual way of energy transfer into the system. Quite expectedly, the oscillatory tail is almost insignificant in the case of the rectangular and exponential loads since the greater part of the energy is concentrated in an intense pulse of short duration. All these observations suggest that the shape of the impulse is a determining factor in the severity of vibration, the sudden discontinuous load being the most critical from the viewpoint of possible structural damage or instability.

Subsequently, the influence of boundary restraints and the elastic foundation on the dynamic behavior of the system is investigated. The time histories of displacement, velocity, and acceleration and the phase diagram under a half-sine impact load are plotted in Figure 8 for the case without an elastic foundation, and in Figure 9 for the case with an elastic foundation for SSSS boundary condition. The results for CFFF boundary condition and CFCF boundary condition without elastic foundation and with considering elastic foundation are demonstrated in Figure 10 to Figure 13.

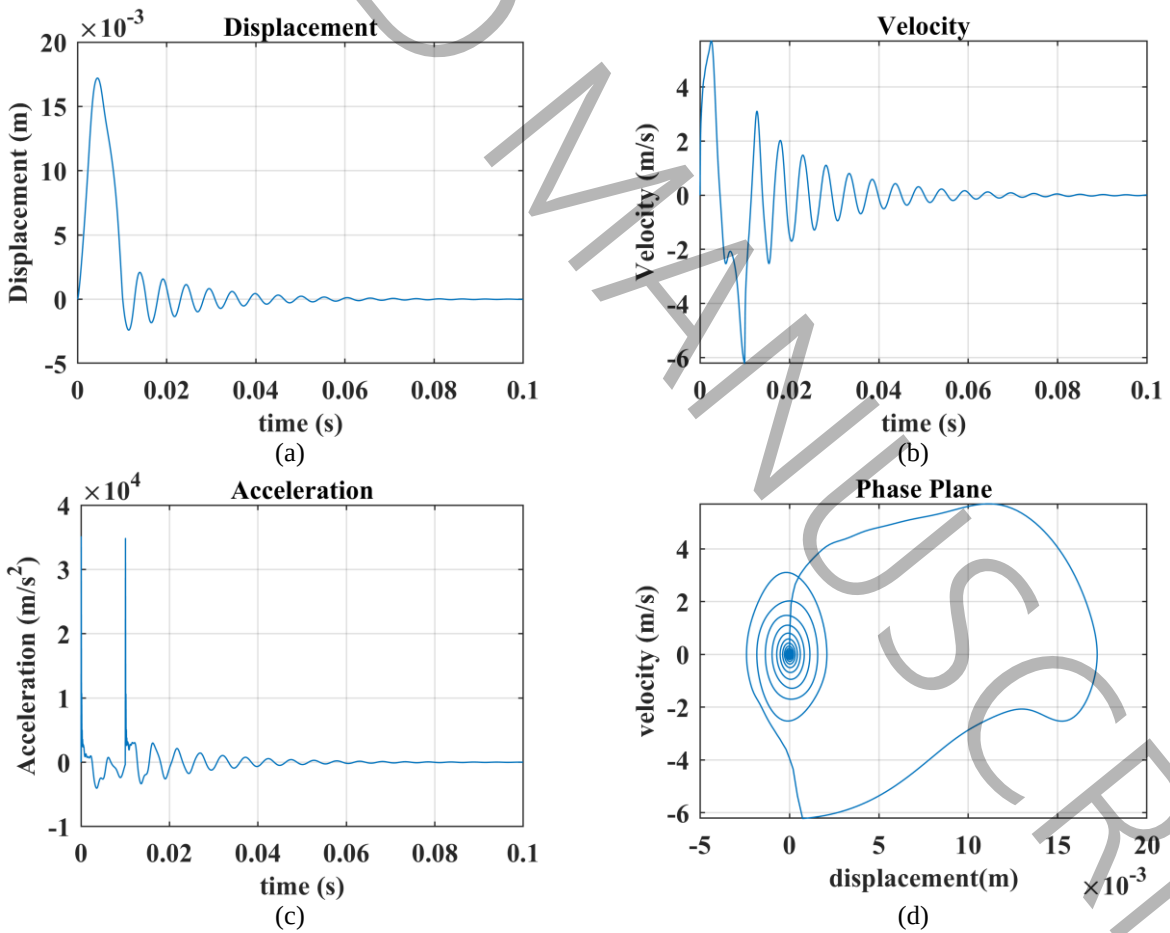

Figure 8. (a) structural displacement, (b) corresponding velocity, (c) acceleration response, and (d) phase portrait for the SSSS boundary condition without an elastic foundation under a half-sine impact load.

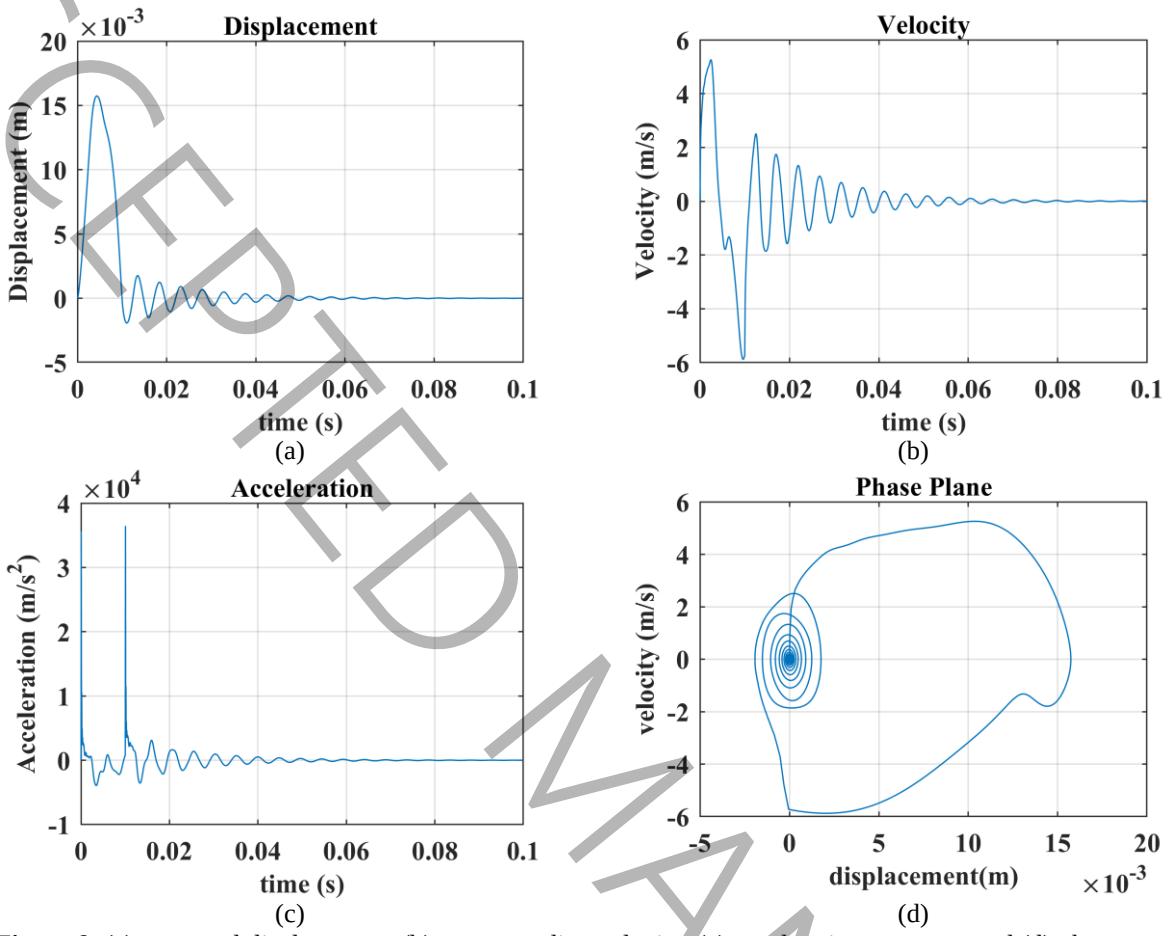

Figure 9. (a) structural displacement, (b) corresponding velocity, (c) acceleration response, and (d) phase portrait for the SSSS boundary condition with an elastic foundation ($K_f = 10^5$ N / m) under a half-sine impact load (ok)

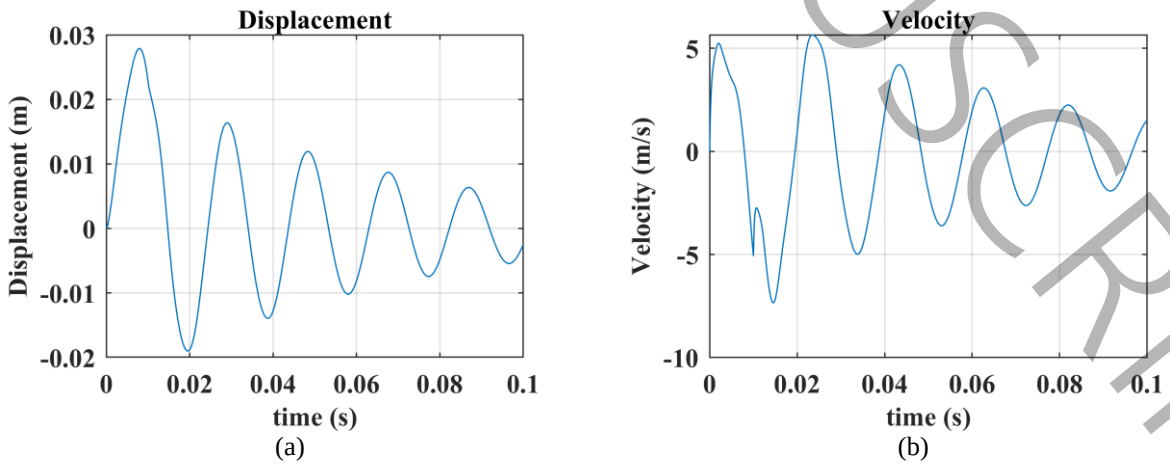

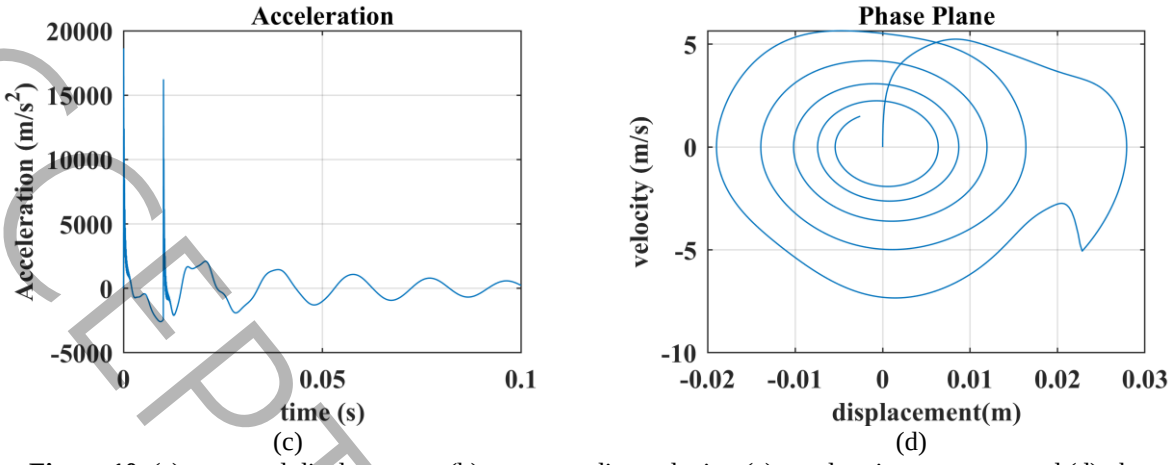

(c) (d)

Figure 10. (a) structural displacement, (b) corresponding velocity, (c) acceleration response, and (d) phase portrait for the CFFF boundary condition without an elastic foundation under a half-sine impact load.

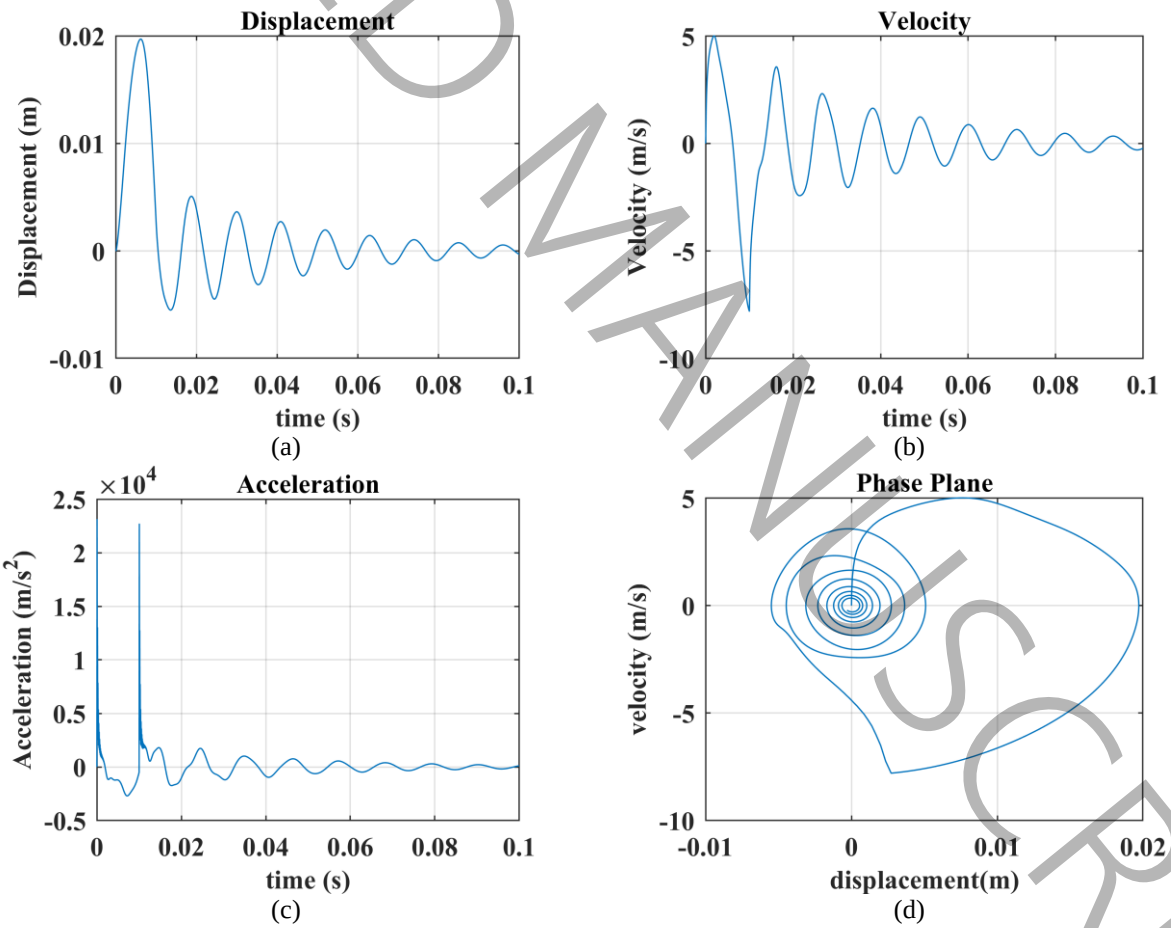

(a) (b)

(c) (d)

Figure 11. (a) structural displacement, (b) corresponding velocity, (c) acceleration response, and (d) phase portrait for the CFFF boundary condition with an elastic foundation ($K_f = 10^5 \text{ N / m}$) under a half-sine impact load

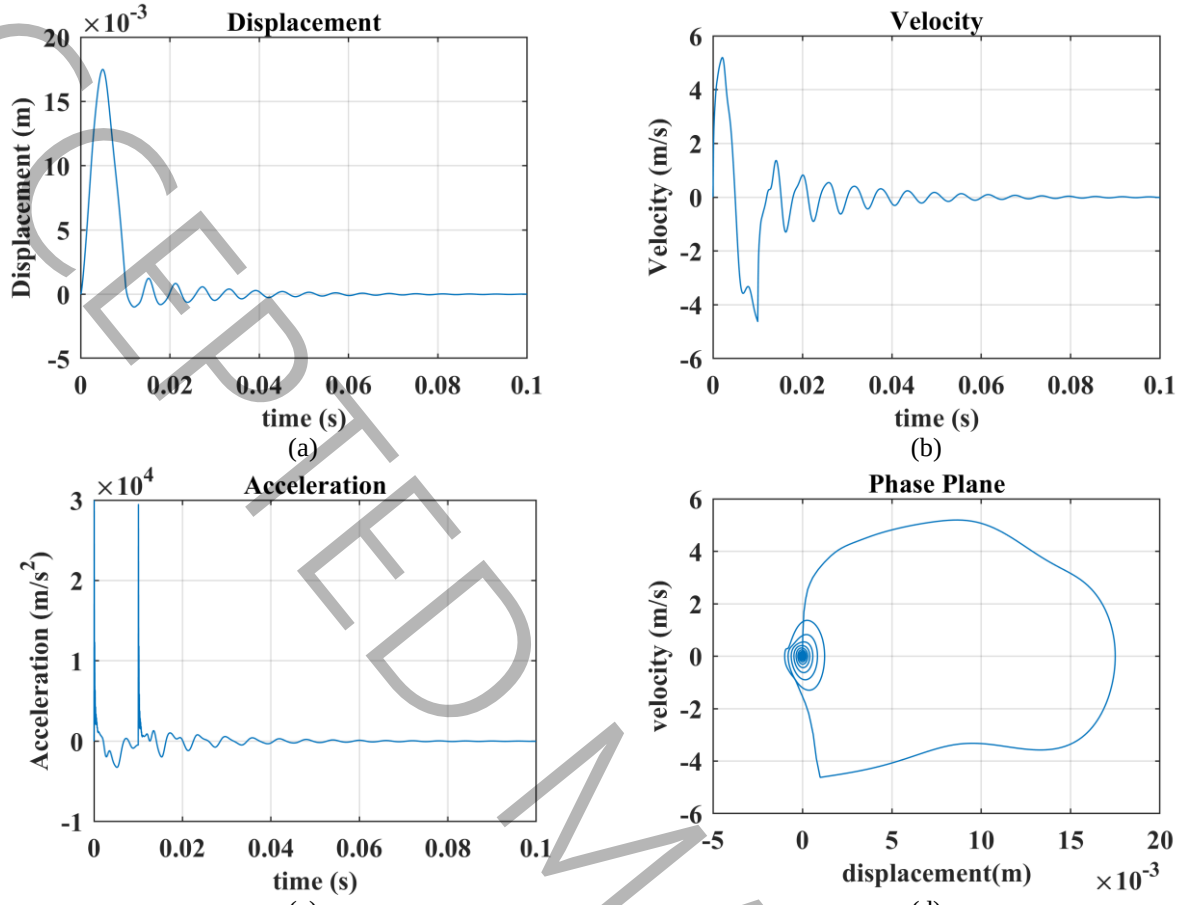

Figure 12. (a) structural displacement, (b) corresponding velocity, (c) acceleration response, and (d) phase portrait for the CFCF boundary condition without elastic foundation ($K_f = 0$) under a half-sine impact load

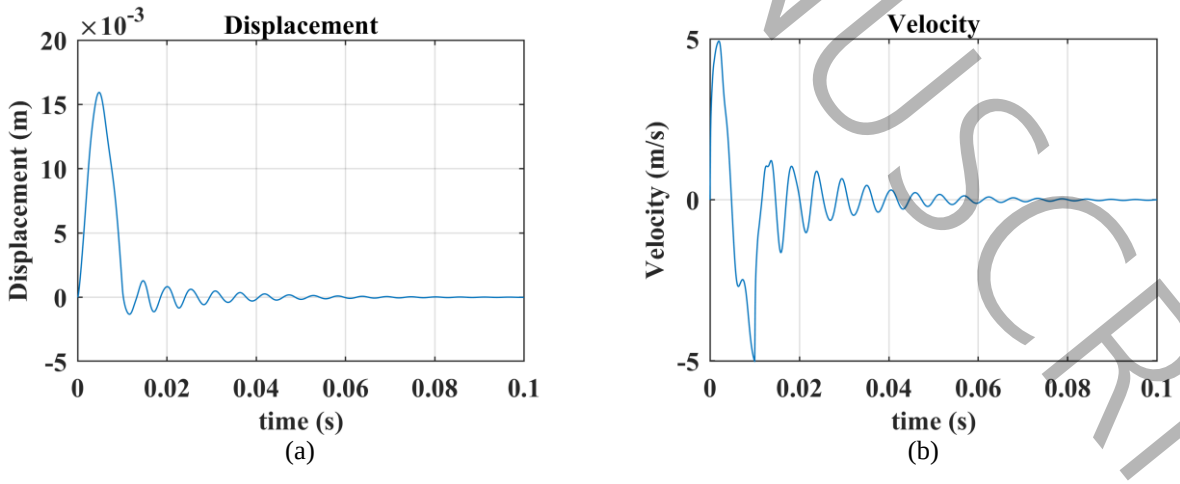

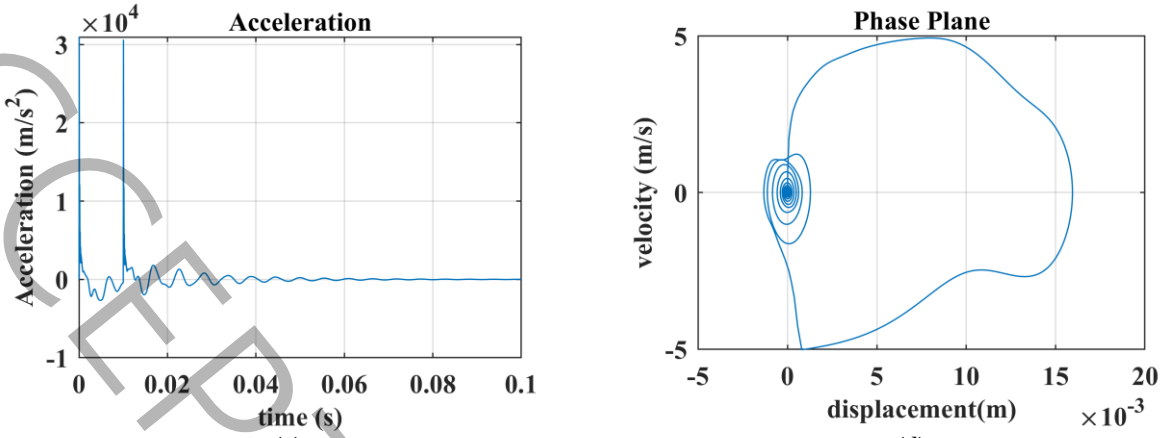

(c) (d)

Figure 13. (a) structural displacement, (b) corresponding velocity, (c) acceleration response, and (d) phase portrait for the CFCF boundary condition with an elastic foundation ($K_f = 10^5 \text{ N/m}$) under a half-sine impact load

The results of the time history and phase diagrams under different boundary conditions (SSSS, CFFF, and CFCF) with and without the elastic foundation reveal that both boundary stiffness and foundation support significantly influence the dynamic response. Fully simply supported conditions and elastic foundation led to increased system stiffness, reduced peak displacements, and faster stabilization. In contrast, more flexible boundaries or the absence of an elastic foundation result in larger oscillations, prolonged response durations, and more pronounced dynamic effects. Phase diagrams further confirm these findings, where closed and tight trajectories are associated with stiffer and more stable configurations, whereas open or spiral paths indicate lower damping and higher energy retention in the system.

6. Conclusion

This work investigates the free and forced vibration behavior of doubly-curved spherical composite sandwich panels incorporating soft cores, resting on elastic foundations and subjected to a range of boundary conditions and impact loading scenarios. A key novelty of the present study is the development of a novel finite element formulation specifically designed to handle impact analysis of open spherical sandwich panels with soft cores on elastic foundations—an area that has remained unexplored in existing research on doubly-curved shells. The findings indicate that increased in-plane stiffness, characterized by higher material property ratios, leads to greater overall structural stiffness and a corresponding rise in natural frequencies. The elastic foundation notably influences both free and forced responses by enhancing the system's stiffness, reducing displacement amplitudes, and accelerating the stabilization of the structure. Additionally, the phase diagrams illustrated that the system exhibits more stable and dissipative behavior with higher boundary restraint and foundation support. On the other hand, rectangular impacts generated the most severe response with higher peak displacements than gradual loads, dangerous acceleration spikes, and prolonged stabilization time, while gradual loads showed superior performance, smooth transitions with lower velocity peaks, and effective energy dissipation. The proposed higher-order element model effectively captures the complex dynamic response of the structure. The model demonstrates accuracy and efficiency in forecasting the vibrational response of curved sandwich panels under dynamic impact loading. Several extensions can be considered in the future studies, such as the inclusion of nonlinear and large-amplitude dynamic effects, alternative or graded core arrangements for enhanced impact resistance, and analyses under more realistic loading conditions, like random or multi-directional or blast-type impulses. Further developments may incorporate thermo-mechanical or hygro-thermal effects, progressive damage and failure modelling, geometric and foundation parameter optimisation, and experimental verification using fabricated spherical panel prototypes. These would extend the utility of the current formulation and provide further understanding of dynamic performance of sandwich shell structures used in aerospace, protective, and industrial applications.

References

[1] V. Birman, G.A. Kardomateas, Review of current trends in research and applications of sandwich structures, Composites Part B: Engineering, 142 (2018) 221-240.
[2] F. Rubino, A. Nisticò, F. Tucci, P. Carlone, Marine application of fiber reinforced composites: A review, Journal of Marine Science and Engineering, 8(1) (2020) 26.
[3] B. Castanié, C. Bouvet, M. Ginot, Review of composite sandwich structure in aeronautic applications, Composites Part C: Open Access, 1 (2020) 100004.
[4] E. Ventsel, T. Krauthammer, E. Carrera, Thin plates and shells: theory, analysis, and applications, Appl. Mech. Rev., 55(4) (2002) B72-B73.
[5] S. Mirza, A.V. Singh, Free vibration of deep spherical sandwich shells, Journal of Engineering Mathematics, 8(1) (1974) 71-79.
[6] H. Biglari, A. Jafari, Static and free vibration analyses of doubly curved composite sandwich panels with soft core based on a new three-layered mixed theory, Proceedings of the Institution of Mechanical Engineers, Part C: Journal of Mechanical Engineering Science, 224(11) (2010) 2332-2349.
[7] S. Hosseini-Hashemi, S.R. Atashipour, M. Fadaee, U.A. Girhammar, An exact closed-form procedure for free vibration analysis of laminated spherical shell panels based on Sanders theory, Archive of Applied Mechanics, 82(7) (2012) 985-1002.
[8] S. Sadripour, R.-A. Jafari-Talookolaei, A. Malekjafarian, An efficient nine-node quadrilateral element for free vibration analysis of deep doubly curved soft-core sandwich shells, Acta Mechanica, 234 (2023) 4111–4145.
[9] T.S. Le, T.T. Tran, C. Pham, Q.H. Pham, Free vibration analysis of functionally graded sandwich spherical shells with honeycomb core resting on Kerr foundation using the MITC4 element, Nondestructive Testing and Evaluation, 40(3) (2025) 1161-1179.
[10] J. Ge, Z. Zhang, Y. Liu, Effect of Graphene Reinforcements on the Natural Frequencies of Metal Foams Sandwich Spherical Panels Situated on Kerr Elastic Foundation Considering Moisture Changes, International Journal of Structural Stability and Dynamics, 25(20) (2024) 2550212.
[11] S. Sahu, R.S. Kumar, Static and free vibration analysis of doubly curved laminated composite shells using Carrera Unified Formulation, Mechanics Based Design of Structures and Machines, (2026) 1-35.
[12] P.M. Culkowski, H. Reismann, The spherical sandwich shell under axisymmetric static and dynamic loading, Journal of Sound and Vibration, 14(2) (1971) 229-240.
[13] V.X. Kunukkasseril, R. Palaninathan, Impact experiments on shallow spherical shells, Journal of Sound and Vibration, 40(1) (1975) 101-117.
[14] M.F. Sahan, Transient analysis of cross-ply laminated shells using FSDT: Alternative formulation, Steel and Composite Structures, 18(4) (2015) 889-907.
[15] A. Wang, H. Chen, W. Zhang, Nonlinear transient response of doubly curved shallow shells reinforced with graphene nanoplatelets subjected to blast loads considering thermal effects, Composite Structures, 225 (2019) 111063.
[16] J. Guo, D. Shi, Q. Wang, J. Tang, C. Shuai, Dynamic analysis of laminated doubly-curved shells with general boundary conditions by means of a domain decomposition method, International Journal of Mechanical Sciences, 138 (2018) 159-186.
[17] A. Dogan, Dynamic response of laminated composite shells under various impact loads, Mechanics of Time-Dependent Materials, (2019) 1-19.
[18] M.G. Kareem, W.I. Majeed, Transient dynamic analysis of laminated shallow spherical shell under low-velocity impact, Journal of Materials Research and Technology, 8(6) (2019) 5283-5300.
[19] P.V. Katariya, S.K. Panda, Numerical evaluation of transient deflection and frequency responses of sandwich shell structure using higher order theory and different mechanical loadings, Engineering with Computers, 35(3) (2019) 1009-1026.
[20] M. Subramani, M. Ramamoorthy, A.B. Arumugam, R. Selvaraj, Free and forced vibration characteristics of CNT reinforced composite spherical sandwich shell panels with MR elastomer core, International Journal of Structural Stability and Dynamics, 21(10) (2021) 2150136.
[21] H. Raissi, Dynamic analysis of a spherical sandwich sector with piezoelectric face sheets and FG-CNT core subjected to low-velocity impact, Journal of the Brazilian Society of Mechanical Sciences and Engineering, 43(7) (2021) 363.
[22] W. Liu, X. Wang, Prediction the Radial Natural Characteristic of Sandwich Spherical Shell Based on Wave Propagation, Journal of Vibration Engineering & Technologies, 12(7) (2024) 8725-8736.
[23] H.N. Thi, Transient Response of Auxetic Honeycomb Sandwich Shell Integrated with Laminated Three-Phase Polymer/GNP/Fiber Face Sheets Subjected to Low-Velocity Impact Load, Journal of Vibration Engineering & Technologies, 13(1) (2025) 71.
[24] S. Sadripour, R.-A. Jafari-Talookolaei, A. Malekjafarian, Dynamic response of open doubly curved sandwich

shells with soft core subjected to a moving force, Acta Mechanica, 235 (2024) 2231–2257.
[25] Y. Frostig, O.T. Thomsen, On the free vibration of sandwich panels with a transversely flexible and temperature-dependent core material–Part I: Mathematical formulation, Composites Science and Technology, 69(6) (2009) 856-862.
[26] S. Sadripour, R.-A. Jafari-Talookolaei, A. Malekjafarian, An efficient nine-node quadrilateral element for free vibration analysis of deep doubly curved soft-core sandwich shells, Acta Mechanica, 234(9) (2023) 4111-4145.
[27] S. Sadripour, R.-A. Jafari-Talookolaei, A. Malekjafarian, Free vibration analysis of deep doubly curved soft-core sandwich panels with different boundary conditions, in: Structures, Elsevier, 2022, pp. 880-901.
[28] B. Khalfi, A. Ross, Transient and harmonic response of a sandwich with partial constrained layer damping: A parametric study, Composites Part B: Engineering, 91 (2016) 44-55.
[29] H. Biglari, A.A. Jafari, High-order free vibrations of doubly-curved sandwich panels with flexible core based on a refined three-layered theory, Composite Structures, 92(11) (2010) 2685-2694.
[30] A.K. Garg, R.K. Khare, T. Kant, Higher-order closed-form solutions for free vibration of laminated composite and sandwich shells, Journal of Sandwich Structures & Materials, 8(3) (2006) 205-235.
[31] A. Nayak, R. Shenoi, S. Moy, Transient response of composite sandwich plates, Composite Structures, 64(3-4) (2004) 249-267.